Author Manuscript

Author Manuscript

Author Manuscript

Author Manuscript

HHS Public Access

Author manuscript

Neurobiol Dis. Author manuscript; available in PMC 2018 December 01.

Published in final edited form as:

Neurobiol Dis. 2017 December ; 108: 29–44. doi:10.1016/j.nbd.2017.07.020.

Differential Electrophysiological and Morphological Alterations of Thalamostriatal and Corticostriatal Projections in the R6/2 Mouse Model of Huntington's Disease

Anna Parievsky[1,*], **Cindy Moore**[2,*], **Talia Kamdjou**[1], **Carlos Cepeda**[1], **Charles K. Meshul**[2,3], and **Michael S. Levine**[1]

[1]Intellectual and Developmental Disabilities Research Center, Semel Institute for Neuroscience and Human Behavior and the Brain Research Institute, David Geffen School of Medicine, University of California Los Angeles, Los Angeles, California

[2]Research Services, VA Portland Health Care System

[3]Department of Behavioral Neuroscience, Oregon Health & Science University, Portland, Oregon, USA

Abstract

Huntington's disease (HD) is a fatal genetic disorder characterized by cell death of medium-sized spiny neurons (MSNs) in the striatum, traditionally attributed to excessive glutamate inputs and/or receptor sensitivity. While changes in corticostriatal projections have typically been studied in mouse models of HD, morphological and functional alterations in thalamostriatal projections have received less attention. In this study, an adeno-associated virus expressing channelrhodopsin-2 under the calcium/calmodulin-dependent protein kinase IIα promoter was injected into the sensorimotor cortex or the thalamic centromedian-parafascicular nuclear complex in the R6/2 mouse model of HD, to permit selective activation of corticostriatal or thalamostriatal projections, respectively. In symptomatic R6/2 mice, peak amplitudes and areas of corticostriatal glutamate AMPA and NMDA receptor-mediated responses were reduced. In contrast, although peak amplitudes of AMPA and NMDA receptor-mediated thalamostriatal responses also were reduced, the areas remained unchanged due to an increase in response decay times. Blockade of glutamate reuptake further increased response areas and slowed rise and decay times of NMDA responses. These effects appeared more pronounced at thalamostriatal synapses of R6/2 mice, suggesting increased activation of extrasynaptic NMDA receptors. In addition, the probability of glutamate release was higher at thalamostriatal than corticostriatal synapses, particularly in R6/2 mice. Morphological studies indicated that the density of all excitatory synaptic contacts onto MSNs was reduced, which matches the basic electrophysiological findings of reduced amplitudes. There was

Send correspondence to: Michael S. Levine, Ph.D., IDDRC Room 58-258, Semel Institute for Neuroscience and Human Behavior, UCLA School of Medicine, 760 Westwood Plaza, Los Angeles, CA 90095, USA. Tel: (310) 825-7595, Fax: (310) 206-5060, mlevine@mednet.ucla.edu.

*These authors contributed equally.

Publisher's Disclaimer: This is a PDF file of an unedited manuscript that has been accepted for publication. As a service to our customers we are providing this early version of the manuscript. The manuscript will undergo copyediting, typesetting, and review of the resulting proof before it is published in its final citable form. Please note that during the production process errors may be discovered which could affect the content, and all legal disclaimers that apply to the journal pertain.

Author Manuscript Author Manuscript Author Manuscript Author Manuscript

a consistent reduction in the area of spines but little change in presynaptic terminal size, indicating that the postsynaptic spine may be more significantly affected than presynaptic terminals. These results highlight the significant and differential contribution of the thalamostriatal projection to glutamate excitotoxicity in HD.

Keywords

Huntington's disease; thalamus; R6/2; medium-sized spiny neurons; optogenetics; Electron microscopy

INTRODUCTION

Huntington's disease (HD) is a progressive neurodegenerative disorder for which there is currently no cure and few treatments are available (Bonelli and Hofmann, 2007; Fasano et al., 2008; Brusa et al., 2009; Mestre et al., 2009). Patients suffer from chorea (involuntary dance-like movements) in early stages, akinesia in later stages, as well as cognitive and psychiatric disturbances (Harper and Jones, 2002; Bonelli and Hofmann, 2007). HD is caused by an unstable expansion of CAG repeats within exon 1 of the Huntington gene (*HTT*) which results in an elongated polyglutamine stretch near the N-terminal of the huntingtin (Htt) protein (The Huntington's Disease Collaborative Research Group, 1993). Htt is a cytoplasmic protein primarily associated with vesicles and microtubules (DiFiglia et al., 1995; Hoffner et al., 2002). It is involved in transcriptional regulation, intracellular trafficking, cytoskeletal organization, endocytosis, and exocytosis (Velier et al., 1998; Waelter et al., 2001; Li et al., 2003), and it also upregulates the expression of brain derived neurotrophic factor (Zuccato et al., 2001).

The most apparent neuropathology in HD is degeneration of striatal medium-sized spiny neurons (MSNs) and cortical pyramidal neurons (Vonsattel et al., 1985), although cells in other regions such as the thalamus also undergo neurodegeneration (Heinsen et al., 1996; Kassubek et al., 2004; Kassubek et al., 2005). There is evidence that indirect pathway MSNs, i.e., those projecting to the external globus pallidus and expressing dopamine (DA) D2 receptors (D2R) and met-enkephalin (Gerfen et al., 1990; Steiner and Gerfen, 1999), are more susceptible to degeneration than direct pathway, DA D1R-expressing MSNs projecting to the substantia nigra and the internal segment of the globus pallidus (Reiner et al., 1988; Albin et al., 1992; Deng et al., 2004), although both pathways are effected in some HD mouse models (Andre et al., 2011).

The excitotoxicity hypothesis of HD postulates that striatal neurons degenerate due to increased glutamate release (DiFiglia, 1990; Freese et al., 1990; Beal et al., 1993). As the striatum receives glutamatergic projections from two different regions, the cerebral cortex and the thalamus (Huerta-Ocampo et al., 2014; Smith et al., 2014), the potential source of excess glutamate, if indeed it occurs, remains unknown. One reason that has hampered identification is that cortical and thalamic projections are interlaced within the striatum. It also has been reported that, unlike corticostriatal projections which synapse predominantly on dendritic spines (Smith and Bolam, 1990), thalamostriatal projections terminate preferentially on dendritic shafts (Smith and Bolam, 1990; Sadikot et al., 1992; Sidibe and

Author Manuscript Author Manuscript Author Manuscript Author Manuscript

Smith, 1996). However, most of these studies were carried out using non-human primates and not rodents. The principal source of thalamic projections to the dorsolateral striatum in rodents is the centromedian-parafascicular (CM/Pf) nuclear complex but other nuclei also contribute (Berendse and Groenewegen, 1990; Smith et al., 2004).

Differential stimulation of each pathway has been particularly challenging using striatal *in vitro* preparations. Electrophysiological studies have used oblique horizontal slices to activate each pathway separately. However, reports employing this technique have yielded contradictory results, possibly due to species and procedural differences (Smeal et al., 2006; Ding et al., 2008; Smeal et al., 2008) or to the lack of sub-regional specificity (Hunnicutt et al., 2016). With the advent of optogenetics these challenges have been largely overcome (Ellender et al., 2011; Sciamanna et al., 2015; Kolodziejczyk and Raymond, 2016).

The present experiments used optogenetics to separately activate each glutamatergic pathway. We examined alterations of glutamate α-amino-3-hydroxy-5-methyl-4-isoxazolepropionic acid (AMPAR) and N-methyl-D-aspartate receptor (NMDAR)-mediated responses at thalamostriatal and corticostriatal synapses in MSNs from symptomatic R6/2 mice compared with wild type (WT) littermates. In addition, we used immunohistochemistry (IHC) and electron microscopy (EM) to determine changes in glutamate terminals originating from either the cerebral cortex or thalamus making synaptic contact onto either direct or indirect pathway MSNs. Both the presynaptic labeling for the corticostriatal vesicular glutamate transporter 1 (VGLUT1) or the thalamostriatal vesicular glutamate transporter 2 (VGLUT2) and the postsynaptic labeling for D1R or D2R were identified using EM and diaminobenzidine (DAB) IHC, followed by immuno-gold labeling for glutamate.

MATERIALS AND METHODS

Animals

All experimental procedures were performed in accordance with the United States Public Health Service Guide for Care and Use of Laboratory Animals and approved by the Institutional Animal Care and Use Committees at the University of California, Los Angeles (UCLA) and the Portland Veterans Administration Medical Center. Every effort was made to minimize pain and discomfort. Genotyping was performed using polymerase chain reaction of DNA obtained from tail samples, once at weaning and again following electrophysiological recordings or morphological assessments. Electrophysiological data from both males and females were combined since we found no sex differences. For morphological experiments only males were used.

All experiments were conducted in the R6/2 mouse model of HD. Our colony at UCLA is maintained by crossing WT C57BL/6xCBA males with R6/2 ovary-transplanted WT C57BL/6xCBA females (The Jackson Laboratories: Bar Harbor, Maine, USA). CAG repeat lengths were determined by Laragen Inc. (Culver City, CA) and ranged between 145–163 (average 154.9±1, n=19 mice). Mice were used for recordings at 64–87 days of age, when they are fully symptomatic. An additional group of mice was used to identify MSNs of the direct pathway. WT C57BL/6xCBA males (The Jackson Laboratories) expressing DsRed

Author Manuscript Author Manuscript Author Manuscript Author Manuscript

fluorescent protein tDTomato were bred to R6/2 ovary-transplanted WT C57BL/6xCBA females to produce R6/2 D1tomato mice which expressed tDTomato in D1R-containing MSNs. In this group of mice CAG repeats ranged between 148–164 (average 157.2±1.7, n=9). These mice were used for recordings at 60–72 days of age.

Opsin Injection

An adeno-associated virus (AAV2) expressing ChR2(H134R) and enhanced yellow fluorescent protein (eYFP) under the Ca^{2+}/calmodulin-dependent protein kinase type IIα subunit (CaMKIIα) promoter was injected to express ChR2 in the sensorimotor cortex or the CM/Pf nuclear complex, which allowed for specific activation of corticostriatal or thalamostriatal inputs respectively. For injections, mice were anesthetized with isoflurane and placed in a stereotaxic frame. Injections were made with a 33 gauge blunt needle using a Chemyx NanoJet pump. Each injection site received 0.5 μl of virus, infused at 0.2 μl/min. Thalamic injections were performed bilaterally in two regions encompassing the CM/Pf nuclear complex of the thalamus (AP: −2.18, ML +/− 0.7, DV −3.8; and AP: −1.58, ML +/− 0.7, DV −3.8) and also including some adjacent nuclei (central lateral, paracentral, and mediodorsal). Cortical injections were unilateral (AP: +2.22, ML +/− 1.7, DV-1.8) and only the injected hemisphere was used for recordings.

Slice preparation and cell visualization

4–5 weeks after viral injection (to allow for sufficient expression) mice were anesthetized with isoflurane and decapitated. The brain was rapidly removed and placed in ice-cold slicing solution containing (in mM): 208 sucrose, 26 $NaHCO_3$, 1.25 $NaHPO_4$, 10 glucose, 2.5 KCl, 1.3 $MgCl_2$, 8 $MgSO_4$ (pH 7.2; aerated with 95% O_2/5% CO_2; 290–300 mOsm/l). Coronal slices (300 μm) were obtained using a vibratome (Model VT1000 S, Leica Microsystems, Buffalo Grove, IL). To ensure only axons, and not somata, were stimulated in animals injected in the cortex, and to reduce the possibility of stimulating thalamocortical terminals in animals injected in the thalamus, the striatum was isolated in all animals before recording.

Slices were maintained at room temperature in artificial cerebrospinal fluid (ACSF) containing (in mM): 130 NaCl, 3 KCl, 26 $NaHCO_3$, 1.25 $NaHPO_4$, 10 glucose, 2 $MgCl_2$, 2 $CaCl_2$ (pH 7.2; aerated with 95% O2/5% CO2; 290–300 mOsm/l) and allowed to recover for at least 1 h prior to recordings. Cells were visualized with infrared illumination and differential interference contrast optics. MSNs were identified by somatic size and basic membrane properties. Patch pipettes were filled with Cs-methanesulfonate solution containing (in mM): 125 cesium methanesulfonate, 8 HEPES, 9 EGTA, 4 NaCl, 3 KCl, 1 $MgCl_2$, 10 disodium phosphocreatine, 0.1 leupeptin (HCl), 5 MgATP, 1 TrisGTP, (pH 7.2; 270–280 mOsm/l) and biocytin (0.2%) to identify recorded neurons. The Na^+ channel blocker QX-314 chloride (4 μM) was added to the internal solution to block action potentials. After recordings slices were fixed in paraformaldehyde (PFA) and processed for biocytin using standard techniques (Horikawa and Armstrong, 1988) to allow post-hoc identification of the recorded MSNs, as well as visualization of virus expression.

Author Manuscript Author Manuscript Author Manuscript Author Manuscript

Electrophysiological Recordings and Optical Stimulation

After the whole-cell configuration was obtained, basic membrane properties were recorded in voltage-clamp mode at a holding membrane potential (V_{hold}) of −70 mV. Membrane capacitance, input resistance, and decay time constant were measured by applying a 10 mV depolarizing step voltage command and using the membrane test function integrated in pClamp 8.2 or 10.3 (Axon Instruments, Molecular Devices, Sunnyvale, CA). Only data from cells with series resistance values smaller than 30 MΩ, which did not vary more than 20% during the course of the experiment were included. Series resistance (<25 MΩ on average) was not compensated.

To isolate AMPAR-mediated currents the cell was maintained at −70 mV and bicuculline (BIC, 10 μM) was added to block $GABA_A$ receptor-mediated currents. Light pulses (470 nm, 1 ms duration, 30 sec apart) were delivered using a light-emitting diode (CoolLED) and all recordings used a suprathreshold intensity of 10 mW. After 5 trials, the AMPAR antagonist 2,3-dihydroxy-6-nitro-7-sulfamoyl benzo[f]quinoxaline-2,3-dione (NBQX, 10 μM) was bath applied. To record NMDA currents, V_{hold} was stepped to +40 mV to eliminate the Mg^{2+} block of NMDARs and the light stimulus was repeated (3 times, 30 seconds apart). To examine probability of release at presynaptic terminals (Zucker, 1989) a subset of cells underwent a paired-pulse stimulation protocol (75 ms, 100 ms, 200 ms, and 400 ms intervals). This protocol was run at V_{hold} of −70 mV to examine paired-pulse ratios (PPRs). To determine potential alterations of glutamate transporters, NMDA currents before and after bath application of a glutamate transporter blocker (DL-TBOA, 30 μM) were compared in a subset of neurons. To examine if alterations specific to NMDARs containing the NR2B subunit occurred, NMDA currents before and 10 min after bath application of Ifenprodil (1 μM) were compared in another subset of neurons.

Electrophysiological data analysis

Evoked AMPA and NMDA responses were averaged and analyzed offline using Clampfit 10.0 (Axon Instruments, Molecular Devices, Sunnyvale, CA). Peak amplitudes were calculated by measuring the difference in amplitude between the highest absolute value of the response and average baseline. Area was calculated by summing the entire area under the curve, from baseline to baseline. Decay times were calculated by measuring the time the response took to decay from 90% to 10% of the peak amplitude and rise times by calculating the time the response took to rise from 10–90%. For cells that underwent TBOA treatment, the percent change of peak amplitudes, areas, decay and rise times of the NMDAR-mediated response were calculated. NMDA/AMPA peak amplitude ratios also were calculated. The PPR of the AMPA response was calculated by dividing the amplitude of the second response by the amplitude of the first response (both measured from baseline of trace to peak).

Histology

A subset of animals injected with the virus was used for histology only. These animals were perfused with 20 ml of phosphate buffered saline (PBS) and then 60 ml of PFA. Brains were extracted and fixed in PFA, then moved to 15% sucrose PBS solution, and finally to a 30% sucrose PBS solution overnight. Brains were frozen on dry ice and sectioned using a cryostat to prepare 30 μm thick coronal slices of the entire striatum and site of injection. One of

Author Manuscript Author Manuscript Author Manuscript Author Manuscript

every six sections was mounted with mowiol mounting medium and imaged with a Leica MZ FLIII fluorescence stereomicroscope equipped with a Leica DFC3000 G grayscale USB 3.0 microscope camera to visualize viral eYFP expression at the site of injection and in the striatum.

Immunohistochemistry (IHC) and electron microscopy (EM)

Male R6/2 mice (n=9) and WT littermates (n=7), 80–90 days old, were anesthetized with a cocktail of 0.2% ketamine/0.02% xylazine and transcardially perfused with 3 ml of heparin (1000 units/ml) in 0.1M phosphate buffer (pH 7.4), followed by 50 ml of EM fixative [2.5% glutaraldehyde, 0.5% paraformaldehyde, and 0.1% picric acid in 0.1M phosphate buffer; pH 7.4]. Brains were cut in half coronally at the level of the hypothalamus, with both halves then placed in EM fixative in a microwave tissue processor (Pelco BioWave, Ted Pella, Inc.) containing a temperature controlled fixation bath (Thermoelectric Recirculating Chiller: Pelco Steady Temp Pro, Ted Pella Inc.) for a total of 60 min [30 min, 150 watts (W) at 28°C/15 min, 150W at 25°C/15 min, 650W at 25°C]. The tissue was then rinsed and left in 0.1 M phosphate buffer (PB) at 4°C until serially sectioned through the striatum (equivalent to +1.4 to +0.14 mm from Bregma) (Franklin and Paxinos, 2007) at 60 μm using a vibratome (Leica vibratome, Leica Microsystems). Pre-embed IHC of striatal tissue using DAB (Sigma, St Louis, MO) as the chromophore was performed as previously described (Spinelli et al., 2014) using antibodies against the DA D1 receptor (Sigma, St Louis, MO; polyclonal, 1:100 dilution), DA D2 receptor (Millipore, Burlington, MA; polyclonal, 1:50 dilution), VGLUT1 (Synaptic Systems, Gottingen, Germany; polyclonal 1:1000) and VGLUT2 (Synaptic Systems; polyclonal 1:100). Labeling for each antibody was carried out on separate pieces of striatal tissue, as well as double labeling for either the direct (D1) or indirect (D2) pathways, and VGLUT1 and VGLUT2.

Single DAB labeled tissue

Striatal tissue was first exposed to an antigen retrieval solution (sodium citrate pH 6.0 or Tris/EDTA pH 9.0, which is antibody dependent) as previously reported (Walker et al., 2012; Spinelli et al., 2014). The striatal tissue sections were incubated in the microwave for 5 min, 550 watts (W), with the temperature restricted to less than 35°C (all the remaining steps occurred at this temperature) in a vacuum chamber that cycles the pressure down to 20 mm Hg and back to atmosphere repeatedly during this step (cycling vacuum), in either sodium citrate pH 6.0 (D1 and D2 antibodies) or Tris/EDTA pH 9.0 (VGLUT1 and VGLUT2 antibodies). The tissue was then rinsed in 0.1 M PBS for 1 min at 150 W, with the vacuum off, exposed to 0.3% hydrogen peroxide at 150 W for 1 min with the vacuum off, and then rinsed in PBS at 150 W for 2×1 min with the vacuum off. For the striatal sections that were going to be incubated with either the D1 and D2 antibodies alone, the tissue was first incubated with 0.5% Triton X-100 for 5 min, 550 W with the cycling vacuum (the tissue that was incubated with the VGLUT1 and VGLUT2 antibodies was left in PBS only and not exposed to Triton X-100), then exposed to the primary antibody (at the dilutions described above) at 200 W for 36 min and 20 sec under continuous vacuum (20 mm Hg, cycling the magnetron for 2 min on/3 min off/2 min on/5 min off repeating for 36 min/20 sec). The tissue was then rinsed in PB, 2×1 min, at 150 W with the vacuum off, then exposed to the secondary antibody (D1 antibody uses a biotinylated goat anti-rat, 1:50; Jackson

Author Manuscript Author Manuscript Author Manuscript Author Manuscript

ImmunoResearch, West Grove, PA; D2, VGLUT1 and VGLUT2 antibodies use a biotinylated goat anti-rabbit, 1:50; Jackson ImmunoResearch, West Grove, PA) for 16 min at 200 W for the following cycle: 4 min on, 3 min off, 4 min on, 5 min off, all on a continuous vacuum. The tissue was then rinsed in PBS, 1 min, at 150 W with the vacuum off, followed by incubation with imidazole buffer [5% imidazole buffer (0.2M), pH 9.0/16% sodium acetate (0.1M), pH 7.2], then exposed to ABC (Avidin-biotin complex, Vector Elite Kit, 1 μl/ml of solution A and B in working imidazole buffer) for 16 min at 200 W, under continuous vacuum, using the following cycle: 4 min on, 3 min off, 4 min on, 5 min off. The tissue was then rinsed in imidazole buffer, 2×1 min, at 150 W with the vacuum off, and then exposed to DAB (0.5 μg/ml+1.5% hydrogen peroxide) for 10 min and 20 sec, at 200 W with constant vacuum. The tissue was then rinsed in imidazole buffer, 1 min, at 150 W with the vacuum off, followed by PBS, 1 min, at 150 W with the vacuum off. The sections were then stored in buffer until processed for EM (see below).

Double DAB labeled tissue

The striatal sections were first incubated in the microwave for 5 min, 550 W at 35°C (all the remaining steps occurred at this temperature) in a vacuum chamber that cycles the pressure down to 20 mm Hg and back to atmosphere repeatedly during this step (cycling vacuum), in sodium citrate pH 6.0 (antigen retrieval for the D1R and D2R antibodies). The tissue was then rinsed in 0.1 M PBS for 1 min at 150 W, with the vacuum off and then exposed to 0.3% hydrogen peroxide at 150 W for 1 min with the vacuum off. The sections were then rinsed in PBS at 150 W for 2×1 min with the vacuum off, and then exposed to 0.5% Triton X-100 for 5 min, 550 W with cycling vacuum. The tissue was then incubated in the primary antibody (D1R/D2R) at 200 W for 36 min and 20 sec under continuous vacuum (20 mm Hg, cycling the magnetron for 2 min on/3 min off/2 min on/5 min off repeating). The sections were then rinsed in PBS, 2×1 min, at 150 W with the vacuum off. For the second round of labeling, the sections were again incubated in the microwave for 5 min, 550 W with cycling vacuum, in Tris/EDTA pH 9.0 (antigen retrieval for VGLUT1 and VGLUT2 antibodies), rinsed in 0.1 M PBS 2×1 min at 150 W, with the vacuum off, then exposed to the second primary antibody at 200 W for 36 min and 20 sec under continuous vacuum (20 mm Hg, cycling the magnetron for 2 min on/3 min off/2 min on/5 min off repeating). After second exposure to the primary antibody, the tissue processing was completed in the same manner as the single labeled tissue outlined above, except that the secondary antibodies for each marker were combined in a single solution and applied to the tissue. Although both the DA receptor and VGLUT antibody labeling are using DAB as the chromophore, we are assuming that in general for nerve terminals making an asymmetrical (excitatory) synaptic contact, we are focusing on the location of the DA receptors on dendritic spines and the VGLUTs within nerve terminals making an asymmetrical synaptic contact. However, we are well aware that a small percentage of the glutamate nerve terminals are positive for the D2 receptor (Sesack et al., 1994), but these same terminals will most likely be either VGLUT1 or VGLUT2 positive also.

EM processing

Using the same Biowave tissue processor, with the temperature restricted to less than 60°C for all steps, the tissue was exposed to 1% osmium tetroxide (OsO_4) (Electron Microscopy

Author Manuscript Author Manuscript Author Manuscript Author Manuscript

Sciences, Hatfield, PA) in 1.5% potassium ferricyanide (Electron Microscopy Sciences, Hatfield, PA) solution at 100W with vacuum cycling for 13 min (cycling the magnetron for 3 min on/2 min off/3 min on/2 min off/3 min on). The tissue was then rinsed in deionized millipore filtered H_2O (Di H_2O). The OsO_4 was then removed and replaced with Di H_2O, then immediately washed again with fresh Di H_2O in the microwave for 2×40 sec, 150 W, with no vacuum. The tissue was then exposed to 0.5% uranyl acetate (Electron Microscopy Sciences, Hatfield, PA) in Di H_2O at 100W, cycling vacuum, for 6 min (cycling the magnetron for 2 min on/2 min off/2 min on).

Dehydration and infiltration

An increasing gradient (50%, 75%, 90%, 2×100%) of ethanol in the microwave at 150W was used for 40 sec, with no vacuum at any of the steps. This was then followed by a 40 sec, 150W step exposure to 100% propylene oxide (PO)(Electron Microscopy Sciences, Hatfield, PA), with no vacuum. Tissue was then placed in a 1:1 solution of PO and EPON/SPURRS resin (Meshul et al., 1994) for 3 min, 200W cycling vacuum, followed by 5×3 min in 100% resin, 200W, cycling vacuum. The tissue slices were then flat embedded between two sheets of ACLAR (Electron Microscopy Sciences, Hatfield, PA) overnight in a 60°C oven in order for the resin to polymerize. The area of interest was then micro-dissected from the embedded slice and super-glued onto a block to prepare for thin sectioning.

Post-embed immuno-gold electron microscopy was performed using a glutamate antibody (non-affinity purified, rabbit polyclonal; Sigma Chemical Co., St. Louis, MO). Thin sections (60 nm) were cut on an ultramicrotome (Leica EM UC7, Buffalo Grove, Il) along the leading edge of the dorsolateral striatal tissue block, using a diamond knife (Diatome, Hatfield, PA). For each of the WT or R6/2 mice, only one thin section/striatum was examined from the various combinations of immunolabeling: VGLUT1/D1R, VGLUT1/D2R, VGLUT2/D1R and VGLUT2/D2R. The primary glutamate antibody, as previously characterized (Phend et al., 1992), was diluted 1:250 in TBST 7.6 in blocking solution [0.5% bovine serum albumin (BSA)] (Electron Microscopy Sciences, Hatfield, PA). Aspartate (1 mM) was added to the glutamate antibody mixture 24 h prior to incubation with the thin-sectioned tissue to prevent any cross-reactivity with aspartate within the tissue. The secondary antibody was goat anti-rabbit IgG (Jackson ImmunoResearch, West Grove, PA); diluted 1:20 in TBST pH 8.2), tagged with 12 nm gold particles. We previously reported that incubation of the antibody with 3 mM glutamate resulted in no immuno-gold labeling, showing the specificity of the glutamate labeling (Meshul et al., 1994). Photographs (10/animal) were taken on a JEOL 1400 transmission electron microscope (Peabody, MA) of DAB labeled terminals (VGLUT1/VGLUT2) and spines (D1/D2) from a single 100 mesh grid (1 thin section/grid) throughout the neuropil (an area containing the highest numbers of synapses) at a final magnification of ×46,200 by an individual blinded to the experimental groups, using a digital camera (AMT, Danvers, MA). Since the DAB labeling was restricted to the leading edge of the thin-sectioned tissue, only the neuropil showing DAB labeling was photographed.

Author Manuscript Author Manuscript Author Manuscript Author Manuscript

Morphological analysis

Photomicrographs were analyzed using ImagePro software (Media Cybernetics, Rockville, MD) by an individual blinded to the experimental groups. In the striatum, the area of DAB labeled terminals or spines was measured, along with the number of gold particles in either the terminal or spine to determine the density of glutamate immuno-gold labeling. For quantification of glutamate labeling within the nerve terminals, the number of immuno-gold particles located either within, or at least touching the synaptic vesicle membrane (i.e., vesicular pool), the number located outside the synaptic vesicles (i.e., the cytoplasmic pool), and those associated with mitochondria, were counted. The vesicular and cytoplasmic pools were combined since the cytoplasmic pool is very small (<10%) compared to the vesicular pool (Meshul et al., 1999). We have reported that nerve terminals making a symmetrical contact contain GABA (Meshul et al., 1999), the precursor for which is glutamate. Therefore nerve terminals making a symmetrical contact will naturally contain some glutamate immunolabeling and cannot be considered immuno-negative as a way of determining a ratio between glutamatergic and GABAergic terminals (Meshul et al., 1994; Meshul et al., 1999). The metabolic pool is also relatively small and thus unlikely to be a major source of variation in labeling density. Since there are no synaptic vesicles or mitochondria located within the dendritic spines, all gold particles were counted. The density of gold particles/μm^2 of nerve terminal area for the vesicular/cytoplasmic and metabolic pools was determined for each animal and the mean density for each treatment group calculated. Background labeling was determined within glial cell processes and was found to be about 10 immuno-gold-labeled particles/μm^2 (Meshul et al., 1994). This was subtracted from the density of presynaptic and dendritic spine immuno-gold-labeled glutamate within the nerve terminals and postsynaptic labeling within spines. The density of gold particles/μm^2 of nerve terminal or spine area was calculated for each section. In addition, the total number of synaptic contacts per field of view (14 μm^2), on both spines and dendrites, was counted (regardless of whether the terminals or spines were D1, D2, VGLUT1 or VGLUT2 labeled), as well as DAB labeled pre- (VGLUT1/VGLUT2) and/or post-synaptic labeled contacts (D1/D2) to determine any changes in the density of contacts or a shift in the percent of labeled contacts.

Statistics

In the text, values are presented as mean ± standard error of the mean (SEM). Group means were compared using appropriate t-tests (Student's or Welch's t-test) or two-way ANOVAs followed by Bonferroni correction using SigmaStat software (Version 3.5; SPSS, Chicago, IL). Differences were considered statistically significant when $p<0.05$. In tables and figures, * equals $p<0.05$, ** $p<0.01$, and *** $p<0.001$.

RESULTS

Electrophysiological Findings

ChR2 viral injections and axon terminal expression—Mice injected with AAV2-CaMKIIα-ChR2(H134R)-YFP in the motor cortex (4 R6/2 and 5 WT) showed intense fluorescence at the injection site (M2) and in fiber bundles of the dorsolateral striatum (Fig. 1A, B). Comparison of eYFP expression in cortical regions revealed no obvious differences

Author Manuscript Author Manuscript Author Manuscript Author Manuscript

of viral spread between R6/2 and WT mice. Mice injected in the thalamus (6 R6/2 and 6 WT) showed intense fluorescence in the CM/Pf nuclear complex and adjacent nuclei (Fig. 1C). Faint diffuse fluorescence could be seen throughout the entire striatum in brain slices from both genotypes (Fig. 1D). Comparison of eYFP expression at the cortical or thalamic injection sites and striatum for both injection sites revealed no obvious differences of viral spread between R6/2 and WT mice.

MSN membrane properties—Electrophysiological recordings were restricted to the dorsolateral striatum. Membrane properties of MSNs from mice injected in the CM/Pf or cortex were not different and therefore data from both groups were pooled. MSNs from R6/2s showed significantly reduced membrane capacitance and increased input resistance compared to MSNs from WT littermates (Table 1). These results are consistent with previous findings (Klapstein et al., 2001; Cepeda et al., 2003) and suggest that MSNs from R6/2s are smaller in size and contain fewer open channels. The decay time constant (Tau) was not significantly different. Following electrophysiological recordings, slices were processed for biocytin and imaged using a confocal microscope (Fig. 2). Biocytin label (in red) revealed typical MSN morphology. All recorded MSNs examined were surrounded by GFP fluorescence from cortical (Fig. 2A) or thalamic (Fig. 2B) terminals.

AMPA and NMDA responses evoked by corticostriatal activation—AMPAR-mediated currents evoked by corticostriatal stimulation were recorded at V_{hold} of −70mV in the presence of the $GABA_AR$ antagonist, BIC (10 μM) (Fig. 3A). Average current amplitude in MSNs recorded from R6/2s was significantly decreased compared to those from WTs (Welch's t-test, $t_{(25.61)}$= 2.93, $p<0.01$) and area (Welch's t-test, $t_{(29.11)}$=2.78, $p<0.01$). In contrast, no significant differences in average decay times were observed. NBQX (10 μM) was then added to block AMPAR-mediated currents and the voltage holding potential was stepped to +40 mV to isolate NMDAR-mediated currents (Fig. 3B). Similar to alterations observed in AMPAR-mediated currents, NMDAR-mediated currents recorded were decreased in amplitude (Welch's t-test, $t_{(25.66)}$=2.28, $p<0.05$) and area (Welch's t-test, $t_{(24.79)}$=2.98, $p<0.01$), compared to those from WT MSNs. However, in contrast to AMPAR-mediated currents, NMDAR-mediated currents from MSNs of R6/2 mice displayed significantly shorter decay times (Welch's t-test, $t_{(37.63)}$=2.83, $p<0.01$). The distribution of peak amplitudes of AMPAR-mediated currents was significantly different between R6/2 and WT MSNs, with R6/2 MSNs having a smaller probability of large responses (Chi-squared, $x^2(4)=13.94$, $p<0.01$). However, peak amplitude distributions of NMDAR-mediated currents were not different between genotypes.

AMPA and NMDA responses evoked by thalamostriatal activation—Similar to AMPAR-mediated responses evoked by corticostriatal stimulation, mean amplitude of AMPAR-mediated currents evoked by thalamostriatal stimulation were significantly decreased in MSNs from R6/2 compared to WT mice (Fig. 3C). Areas of AMPA currents were similar between genotypes while decay times were significantly slower (Welch's t-test, $t_{(28.61)}=-3.40$, $p<0.01$) in R6/2 compared to WT MSNs. Average amplitudes and areas of NMDAR-mediated currents were similar in R6/2 and WT MSNs (Fig. 3D). However, similar to the alteration observed when comparing AMPAR-mediated currents, NMDAR-

Author Manuscript Author Manuscript Author Manuscript Author Manuscript

mediated currents recorded in R6/2 MSNs had slower decay times than those recorded in WT MSNs (Welch's t-test, $t_{(53.88)}=-2.22$, $p<0.05$). In addition, similar to differences observed in cortically evoked AMPAR-mediated currents, the distributions of peak amplitudes of thalamically-evoked AMPAR-mediated currents were significantly different between genotypes. R6/2 MSNs showed a smaller probability of large responses (Chi-squared, $x^2(4)=12.00$, $p<0.05$). Distributions of NMDAR-mediated currents were similar between genotypes.

A closer look at the decay times of AMPAR-mediated responses in mixed populations of MSNs (D1 and D2 receptor-expressing) from R6/2 mice revealed a bimodal distribution. Taking 50 ms as the cutoff decay time, MSNs could be clearly separated into populations with short (mean±SEM; 33.2±2.6 ms, n=16) and long (91.5±8.7 ms, n=16) decay times, suggesting they could represent MSNs from the direct or indirect pathway. In order to gain further insight into the specificity of changes in decay times evoked by thalamic stimulation we examined responses in MSNs from WT and R6/2 D1 tdTomato-expressing mice. Non-labeled cells were considered to be D2 MSNs. We found that slower decay times for AMPA responses were specific to D1 cells (WT 39.9±8.5 ms *versus* R6/2 77.2±12.4 ms, n=9 and 12 respectively, p=0.025) **(not shown)**. Similarly, slower decay times for NMDA responses were specific to D1 cells (WT 785.7±70.8 ms *versus* R6/2 1016.5±63.4 ms, n=9 and 18 respectively, p=0.026). This indicates that, in addition to changes in glutamate release probability, alterations in thalamostriatal synapses targeting D1 MSNs also occur. This could be due to postsynaptic changes or altered glutamate transport specifically in D1 MSNs.

Effects of glutamate transport inhibition on NMDA responses evoked by cortical and thalamic activation—To examine the mechanism by which decay times of NMDA currents are differentially affected by cortical (reduced) *versus* thalamic (increased) stimulation, we assessed glutamate reuptake at both corticostriatal and thalamostriatal projections by comparing NMDAR-mediated currents before and 14 min after bath application of TBOA (30 μM), a non-selective glutamate transporter blocker with high affinity for glial and neuronal glutamate transporters (Shimamoto et al., 2004). Amplitude, area, rise and decay time of NMDA currents evoked by corticostriatal or thalamostriatal stimulation were measured before and after TBOA application (Fig. 4). NMDA currents evoked by corticostriatal stimulation displayed a slight, non-significant, decrease in average amplitude that was similar in WT and R6/2 mice. Average percent area and rise time were increased, with the increase being more prominent in MSNs from R6/2 than WT mice (Fig. 4A, B). However, only the difference in rise time reached statistical significance (p=0.35 for area and p=0.012 for rise time). NMDA currents evoked by thalamostriatal stimulation showed differential effects in MSNs from R6/2s and WTs when exposed to TBOA (Fig. 4C, D). The blocker had minimal effects on amplitude but equal increases in decay time of NMDA currents evoked in both R6/2 and WTs. Average area and rise time were increased in MSNs from R6/2s and WTs, although only the rise time reached statistical significance (p=0.21 for area and p=0.035 for rise time).

These observations indicate that, although glutamate transporter block equally affected decay times in WT and R6/2 mice, the overall area of the NMDA response trended to increase in R6/2 mice due to a combination of slower rise and decay times.

Author Manuscript Author Manuscript Author Manuscript Author Manuscript

Effects of selective blockade of GluN2B-containing NMDARs on responses evoked by cortical and thalamic activation—To examine alterations of GluN2B subunit-containing NMDARs at corticostriatal and thalamostriatal synapses, NMDAR-mediated currents were compared before and after bath application of 1 μM Ifenprodil (Fig. 5). As expected, average amplitude of NMDAR-mediated currents was decreased as early as 5 min after Ifenprodil application, and continued to decrease over time. This was true for NMDAR-mediated currents evoked by activation of both corticostriatal and thalamostriatal projections (Fig. 5B). However, no significant differences on average amplitude, area, or kinetics of MSN responses from R6/2 *versus* WT mice were observed (Fig. 5B, C). Comparison between responses evoked by corticostriatal and thalamostriatal stimulation after Ifenprodil application also did not result in any significant differences, indicating that NMDARs expressing GluN2B subunits were equally distributed on corticostriatal and thalamostriatal inputs to MSNs.

NMDA/AMPA ratios—Absolute amplitudes of AMPAR- and NMDAR-mediated currents are potentially affected by the degree of ChR2 expression. Although no gross differences in viral expression were observed between WT and R6/2 mice, to account for potential differences in viral expression, NMDA/AMPA ratios were calculated. The amplitude of the NMDAR-mediated current was divided by the amplitude of the AMPAR-mediated current. The NMDA/AMPA ratios for each neuron were then averaged within their appropriate group (WT *versus* R6/2, and thalamostriatal *versus* corticostriatal stimulation).

NMDA/AMPA amplitude ratios of responses evoked by corticostriatal stimulation were similar between MSNs from R6/2 and WT mice (Fig. 6A, left and right panel). To further assess differences in relative contributions of thalamostriatal and corticostriatal inputs to MSNs NMDA/AMPA amplitude ratios at corticostriatal *versus* thalamostriatal projections were compared. For both MSNs from WT and R6/2 mice, thalamostriatal projections had larger amplitude NMDA/AMPA ratios compared to corticostriatal projections (Fig. 6B). This difference was due to larger NMDA currents at thalamostriatal compared to corticostriatal inputs. This finding agrees with previously published data reporting larger NMDA/AMPA ratios at thalamostriatal than corticostriatal projections (Smeal et al., 2008).

Paired-Pulse Ratios—To examine the probability of neurotransmitter release at corticostriatal and thalamostriatal projections, we used a paired-pulse protocol (Zucker, 1989) in a selected population of MSNs. The paired-pulse protocol was administered in the presence of BIC (10 μM) and V_{hold} of −70 mV to isolate AMPAR-mediated currents. In MSNs from both WT and R6/2 mice, cortical stimulation paired-pulse depression of AMPAR-mediated currents occurred at short inter-pulse intervals (75 and 100 ms), whereas at longer intervals (200 and 400 ms) the depression was reduced (Fig. 7A, B). Results of the paired-pulse stimulation of thalamostriatal projections yielded different outcomes. MSNs from both WT and R6/2 mice displayed paired-pulse depression of AMPAR-mediated responses. However, the depression was significantly larger at 100–400 inter-pulse intervals for R6/2 mice (Fig. 7C, D), suggesting increased probability of glutamate release at thalamostriatal projections compared to WT mice. In summary, compared to WTs, R6/2s

Author Manuscript Author Manuscript Author Manuscript Author Manuscript

display an increased probability of release at thalamostriatal projections, and no change in probability of release at corticostriatal projections.

Morphological Findings

In order to gain insight into the structural bases underlying functional alterations in synaptic transmission, we undertook a series of morphological studies taking advantage of methods that allow separation of corticostriatal (VGLUT1 expression) and thalamostriatal (VGLUT2 expression) inputs, as well as of postsynaptic direct (D1R-expressing) and indirect (D2R-expressing) pathway MSNs. In addition, glutamate immuno-gold labeling provided an estimate of the relative glutamate density in nerve terminals originating from either the cortex (VGLUT1) or thalamus (VGLUT2) and in pre- and postsynaptic terminals of direct and indirect pathway MSNs. For these studies we separately analyzed EM photomicrographs with different combinations of immunolabeling. These included combined labeling for D1R-VGLUT1, D1R-VGLUT2, D2R-VGLUT1 and D2R-VGLUT2 (Figs. 8, 9). For each set of photomicrographs we analyzed the total number of synaptic contacts per field of view, the number of labeled contacts per field of view and the percent change of labeled contacts (Fig 10). Due to the methodology used for this analysis, the data most likely underestimate the change in the number of synaptic contacts per volume (μm^3) in the neuropil within the dorsolateral striatum since stereological methods were not carried out. We also analyzed the areas of the presynaptic terminal and the postsynaptic spine (Fig. 11) and we determined the density of glutamate immuno-gold particles in each set of presynaptic terminals and postsynaptic spines (Fig. 12). Electron photomicrographs clearly showed single DAB labeling for D1R and D2R primarily within spines and VGLUT1 and VGLUT2 labeling within nerve terminals along with nerve terminal glutamate immuno-gold labeling (Figs. 8, 9).

We first determined the density of asymmetrical synaptic contacts per field of view using non-stereological methods. There were significant decreases in the density of synaptic contacts/14 μm^2 in all sets of photomicrographs when comparing the R6/2 vs WT groups (Fig. 10A). Similarly, the number of labeled contacts was decreased in all sets of photomicrographs but these differences were statistically significant only for D1R-VGLUT1 and D2R-VGLUT2 terminals (Fig. 10B). However, the percent of labeled contacts was not significantly decreased (and one, D1R-VGLUT2, was actually significantly increased) for any of the groups indicating that many of the decreases were simply accounted for by the initial difference in total number of synaptic contacts (Fig. 10C). There were almost no significant changes in presynaptic terminal areas (except for a significant decrease in D1R-VGLUT2-expressing terminals) (Fig. 11A). In contrast, all spine areas were reduced in the R6/2 mice and the reduction was statistically significant for both D1R-VGLUT1 and D1R-VGLUT2 spines (Fig. 11B). Although the areas of D2R-labeled spines making contact with just VGLUT1- or VGLUT2-labeled terminals also were decreased, the differences did not reach statistical significance. When we examined the number of gold particles in terminals we found significant reductions within terminals contacting D1R-positive spines but not D2R-positive spines (Fig. 12A). However, the densities of glutamate particles were significantly reduced for cortical inputs contacting both D1R- and D2R-expressing spines (Fig. 12B). The numbers of gold particles in spines contacted by cortical inputs were

Author Manuscript Author Manuscript Author Manuscript Author Manuscript

statistically significantly reduced (Fig. 12C), but there were no significant differences in density of glutamate particles in spines (Fig. 12D). The percentage of VGLUT1 or VGLUT2 positive nerve terminals contacting either a D1R- or D2R-labeled spine versus a D1R- or D2R-labeled dendritic shaft in the WT compared to the R6/2 mice was determined. We found that, for VGLUT1 or VGLUT2 labeled terminals contacting spines, the percentage of VGLUT1/D1R (WT 90.8±2.8, R6/2 81.8±7.6), VGLUT1/D2R (WT 93.2±1.5; R6/2 93.8±0.3), VGLUT2/D1R (WT 84.8±4.9; R6/2 82.9±4.7), and VGLUT2/D2R (WT 91.5±2.1; R6/2 85.2±5.2) labeled tissue showed that the vast majority of terminals originating from either cortex or thalamus were contacting spines. None of the values were statistically different between WT and R6/2 mice or between the four variously labeled groups. Only a small percentage of the VGLUT1 or VGLUT2 labeled terminals (~10–15%) contacted dendritic shafts and none of the immunolabeled groups were statistically different from each other (data not shown).

Together, these findings indicate that the density of all excitatory synaptic contacts onto MSNs is reduced, which matches the basic electrophysiological findings of reduced amplitudes. The consistent reduction in area of spines coupled with the lack of change in presynaptic terminal size indicates postsynaptic spines may be more significantly affected than the remaining presynaptic terminals.

DISCUSSION

Selective activation of distinct axonal projections using optogenetics allowed extensive examination of cortical and thalamic projections into the striatum and demonstrated that these excitatory convergent inputs undergo similar but also differential alterations in HD. The peak amplitude and area of AMPAR- and NMDAR-mediated responses evoked by cortical stimulation were reduced. Although AMPA responses evoked by thalamic stimulation also were reduced, the absolute areas were not affected. This was due to a significant increase in decay time at thalamostriatal synapses for both AMPA and NMDA responses. This could be a compensatory mechanism to ensure faithful thalamostriatal communication. Interestingly, decay times of NMDA responses were reduced at corticostriatal synapses. Blockade of glutamate transporters with TBOA demonstrated a slowdown of NMDA current deactivation kinetics which was similar in both genotypes, and a trend toward increased areas due to slower rise and decay times. Overall, these effects were more pronounced in cells from R6/2 mice and more evident at thalamostriatal synapses. Further supporting thalamic involvement in HD alterations, PPR data suggested increased probability of glutamate release from thalamic inputs to MSNs from R6/2s compared to WTs. Thalamic and cortical projections utilize distinct vesicular glutamate transporters (Fremeau et al., 2001; Herzog et al., 2001; Lei et al., 2004). Thus, differential effects of mHtt on VGLUT2 and VGLUT1 may be in part responsible for the distinct changes of postsynaptic responses observed at thalamostriatal and corticostriatal projections respectively. Data from Ifenprodil experiments did not support alterations in subunit composition of NMDARs, specifically in the proportion of NMDAR-containing GluN2B subunits.

Author Manuscript Author Manuscript Author Manuscript Author Manuscript

Neurodegeneration of the striatum in HD involves a complex interplay of intrinsic, presynaptic, and postsynaptic mechanisms. According to a classic notion, altered cortical input is the main culprit of striatal neurodegeneration (DiFiglia, 1990; Cepeda et al., 2007). With the recognition that thalamic input to the striatum is as important as cortical input, the need to elucidate the source(s) of altered glutamate release became peremptory. However, due to the complex and heterogeneous organization of the striatum, this task had been extremely challenging. Optogenetics has allowed, for the first time, examination of alterations in thalamostriatal and corticostriatal projections in HD separately. Based on previous data showing decreased synaptic communication along the corticostriatal pathway in R6/2 mice (Klapstein et al., 2001; Cepeda et al., 2003; Joshi et al., 2009; Cummings et al., 2010), we expected to see changes in the amplitude of glutamate receptor-mediated currents. In agreement with this prediction, the amplitude and area of responses evoked by cortical stimulation were significantly decreased. In addition, we now demonstrate that thalamic input also is reduced. However, the change in area was not statistically significant due to increases in decay time.

We also found that MSNs from both WT and R6/2 mice displayed paired-pulse depression of AMPAR-mediated responses. This result is consistent with previously published data which found that thalamostriatal synapses display a high probability of release to an initial stimulus which declines rapidly with successive stimulation (Ding et al., 2008), a very fitting property for the role of thalamostriatal projections in transmitting precisely timed signals. However, we also found that in R6/2 mice the depression was more prominent. Perhaps the increased release of glutamate at thalamostriatal synapses in HD mice is a compensatory mechanism to make up for the loss of thalamic inputs.

The contribution of glutamatergic receptors at thalamostriatal *versus* corticostriatal synapses in physiological conditions has been disputed (Ding et al., 2008; Smeal et al., 2008). Whole-cell slice recordings from mouse brains suggested that NMDARs mediate larger currents than AMPARs at corticostriatal projections, while NMDAR-mediated currents are smaller than AMPAR-mediated currents at thalamostriatal projections. In other words, NMDA/AMPA ratios are greater for corticostriatal than thalamostriatal projections (Ding et al., 2008). However, whole-cell slice recordings from rat brains suggested that the NMDA/AMPA ratio was greater for responses evoked from thalamostriatal projections than for those evoked from corticostriatal projections (Smeal et al., 2008). Comparison of NMDA/AMPA ratios in the present study suggested a larger contribution of NMDARs at thalamic inputs compared to cortical inputs. This was true for both R6/2 and WT mice. A higher relative proportion of NMDARs at thalamostriatal synapses, longer decay times of NMDAR-mediated currents, and increased glutamate release probability, all support an important role of thalamostriatal projections in excitotoxicity.

One of the key recurrent findings of our study was altered decay times of glutamate receptor-mediated currents caused by changes in glutamate receptor subunit composition or by deficits in glutamate reuptake, which has been consistently found in HD. Postsynaptic changes in receptor subunit composition would be expected to result in unique changes to AMPAR- *versus* NMDAR-mediated currents. Since both AMPAR- and NMDAR-mediated currents evoked by thalamostriatal stimulation display longer decay times, this change is less

Author Manuscript Author Manuscript Author Manuscript Author Manuscript

likely to occur due to alterations in receptor subunit composition. Therefore, we hypothesize that the observed increase in decay times is occurring as a result of vesicular and/or glutamate transporter changes and is probably specific for D1 MSNs. Postmortem HD tissue shows a reduction of GLT1 and decreased glutamate reuptake (Arzberger et al., 1997; Hassel et al., 2008; Faideau et al., 2010). Failure in glutamate reuptake and the resulting excitotoxicity also have been proposed in HD models (Lievens et al., 2001; NicNiocaill et al., 2001; Miller et al., 2008; Estrada-Sanchez et al., 2009; Tong et al., 2014; Dvorzhak et al., 2016), however, see (Parsons et al., 2016). Further, mutant *HTT* expression restricted to astrocytes is sufficient to decrease GLT1 levels and elicit the HD behavioral phenotype (Bradford et al., 2009). In support, R6/2 mice treated with ceftriaxone show increased striatal GLT1 expression, increased glutamate uptake and, importantly, improvement in some HD behavioral deficits (Miller et al., 2008). In summary, consistent evidence shows a link between altered glutamate reuptake and excitotoxicity in HD.

In a recent study, thalamostriatal and corticostriatal synapses were examined in the YAC128 HD model at a presymptomatic stage (2–3 mo) using similar procedures as in the present study. Similar to our results, an increased contribution of NMDARs and increased probability of release at thalamic compared to cortical synapses were found, and these changes were more evident in YAC128 mice (Kolodziejczyk and Raymond, 2016). Furthermore, a larger contribution of extrasynaptic NMDARs, as evidenced by TBOA application, also was found in both studies and this occurred at both corticostriatal and thalamostriatal synapses of HD mice. However, in Kolodziejczyk and Raymond's study the change was due to increased decay times whereas in our study the effect appeared due to a combination of increased rise and decay times. It is possible that, in our HD model, we did not see a genotype-specific increase in decay time because NMDA responses evoked by thalamostriatal terminal activation displayed increased decay times even before TBOA application (see Fig. 3D), probably resulting in a ceiling effect. Finally, in contrast to our findings, AMPA and NMDA response amplitudes evoked by optical stimulation were not significantly different in YAC128 mice compared to WTs. This can be probably explained by the existence of biphasic changes in glutamate transmission during phenotype progression in HD mouse models (Cepeda et al., 2003; Graham et al., 2009; Joshi et al., 2009).

Overall, electrophysiological data were supported by morphological measurements using quantitative ultrastructural IHC. Reduced responses to cortical and thalamic stimulation can be explained by a generalized decrease in the number of total asymmetric synaptic contacts/field of view (14 μm^2) in R6/2 *versus* WT mice. In addition, spine area also was reduced and this effect was more prominent in D1R-positive spines. This contrasts with the classic idea that, in HD, MSNs of the indirect pathway are more affected than those of the direct pathway (Reiner et al., 1988; Albin et al., 1992). Cortical or thalamic terminal areas were not different between genotypes, except for a significant decrease in size of VGLUT2 terminals contacting D1-labeled spines in the R6/2 compared to the WT group. Interestingly, there was a concomitant increase in the percentage of VGLUT2 labeled terminals contacting D1R-positive spines, suggesting ongoing compensatory mechanisms to counter for reduced thalamic input. We also found a decrease in the density of glutamate immuno-gold labeling within all labeled (VGLUT1 and VGLUT2) nerve terminals contacting either D1- or D2-

Author Manuscript Author Manuscript Author Manuscript Author Manuscript

labeled spines, but only the terminals originating from the cortex (VGLUT1) were significantly different in the R6/2 compared to the WT mice. This probably means that in HD, glutamate density within corticostriatal terminals is more affected than thalamostriatal input and/or that compensatory mechanisms in the cortex are less robust.

In the CAG140 HD mouse model, at the one month time period, it was reported that there was a 20% decrease of VGLUT2 axospinous contacts and a 40% decrease in the VGLUT2 contacts onto dendrites compared to the wildtype mice (Deng et al., 2013). The VGLUT2 axospinous loss persisted out to 12 months of age, suggesting early and persistent involvement of thalamostriatal synapses in changes of glutamate transmission. In addition, there was a 30% loss of VGLUT1 labeled terminals at the 12 month time period. A similar decrease in VGLUT2 terminals contacting cholinergic interneurons within the striatum was reported recently (Deng and Reiner, 2016). This decrease in the overall excitatory input to the striatum is also in agreement with previous reports using an additional slowly progressing HD mouse model, the YAC128 (Singaraja et al., 2011). In that report there was no differentiation between the corticostriatal and thalamostriatal afferents. In the current study, we did find a decrease in the overall density of axospinous synaptic contacts in the R6/2 compared to the WT group, which would be in agreement with Deng et al. (2013). In addition, the decrease in the area of the VGLUT2 labeled terminals in the R6/2 *versus* WT is consistent with Deng et al. (2013). However, further detailed morphological characterization in the current study showed this decrease occurred for VGLUT2 labeled terminals contacting just D1 labeled spines and not D2 spines. We report no change in the area of the VGLUT1 labeled terminals in the R6/2 mice, which is in contrast to the decrease found after 4 or 12 months in the CAG140 HD mouse model (Deng et al., 2013). In addition, we report an increase in the percentage of VGLUT2 labeled terminals making contact with D1-labeled spines in the R6/2 compared to the WT group. However, the current study double labeled for both the presynaptic terminal (VGLUT2) and the postsynaptic spine (D1) compared to Deng et al. (2013), which may account for the difference in our respective findings.

Anatomo-Physiological Considerations

There are time-dependent changes in the excitatory input to the striatum that differentially affect both the direct and indirect pathway MSNs in HD mouse models (Cepeda et al., 2003; Andre et al., 2011; Raymond et al., 2011; Galvan et al., 2012). There are increases in excitatory input to primarily the D1 MSNs early on in the disease process followed by a decrease in this excitatory input to both the D1 and D2 MSNs late in the progression of the disease (Andre et al., 2011; Galvan et al., 2012). The ultrastructural data agree with the effect primarily on the D1-labeled spines associated with the direct pathway but we also observed some changes in D2-labeled spines of the indirect pathway MSNs. In addition, we found that nearly 90% of VGLUT1-labeled terminals in the mouse synapse on spines, regardless of whether the spine was labeled for D1R or D2R. However, we also found that well over 80% of VGLUT2-labeled terminals also synapse on dendritic spines and not on dendritic shafts, in contrast to reports based on non-human primates (Sadikot et al., 1992; Sidibe and Smith, 1996).

Author Manuscript Author Manuscript Author Manuscript Author Manuscript

The decrease in excitatory input that occurs late in the disease process may be associated with ultrastructural changes in either the presynaptic density of glutamate immuno-gold labeling or in the size of the dendritic spine. In the current study we report a decrease in nerve terminal glutamate immuno-gold labeling in the R6/2 *versus* WT mice. Although in the early stages of the disease in the HD mouse models there is evidence for increased excitatory input to the striatum (i.e., possible increased glutamate release), this reverses in the later stages of the disease. At the ultrastructural level, the depletion of nerve terminal glutamate immuno-gold labeling in the R6/2 *versus* WT mice may be a consequence of the earlier increased excitatory input to the striatum. In preliminary studies of layer II of the motor cortex, we also find a similar decrease in the density of glutamate immunogold labeling in VGLUT1 positive nerve terminals (i.e., cortico-cortical contacts) between the R6/2 *versus* WT mice (unpublished findings). In addition, there was a decrease in the overall density of synaptic contacts/field of view (14 μm^2), which affected both VGLUT1-labeled terminals contacting D1R labeled spines and VGLUT2-labeled terminals contacting D2R labeled spines. These data suggest that at the ultrastructural level, changes in presynaptic glutamate immuno-gold and overall synaptic density are associated with the electrophysiological changes previously reported within layer II of the motor cortex (Indersmitten et al., 2015).

Conclusions and Future Perspectives

The differential alterations observed at thalamostriatal compared to corticostriatal projections suggest that the effects of mHtt occurring in the basal ganglia circuit are complex, diverse, and not universal. Therefore, HD treatments aimed at globally decreasing NMDA currents, increasing GLT1 function, or decreasing glutamate release, could result in unfavorable side effects. Treatments designed to target these and other mechanisms altered in HD should be directed to affect specific brain regions, projections, and neuronal types.

Using BACHD and Cre mice, mHtt expression has been reduced in distinct brain regions to study how regional specificity of mHtt affects the HD phenotype. Reduction of mHtt expression in the cortex partially improved the behavioral and psychiatric phenotype but not cell death, reduction of mHtt in the striatum partially rescued the psychiatric phenotype and cell death in the forebrain, while reduction of mHTT in the cortex and striatum simultaneously ameliorated all behavioral deficits and brain atrophy (Wang et al., 2014). It will also be important to examine the effects of mHtt reduction specifically in thalamostriatal projections.

Acknowledgments

We would like to acknowledge the help of Donna Crandall for the illustrations. Support was provided by NIH grant NS41574 and Merit Review #1BX 001643 to CKM from the United States (U.S.) Department of Veterans Affairs Biomedical Laboratory Research and Development. The contents do not represent the views of the U.S. Department of Veterans Affairs or the United States Government.

References

Albin RL, Reiner A, Anderson KD, St Dure L, Handelin B, Balfour R, Whetsell WO Jr, Penney JB, Young AB. Preferential loss of striato-external pallidal projection neurons in presymptomatic Huntington's disease. Ann Neurol. 1992; 31:425–430. [PubMed: 1375014]

Author Manuscript Author Manuscript Author Manuscript Author Manuscript

Andre VM, Cepeda C, Fisher YE, Huynh M, Bardakjian N, Singh S, Yang XW, Levine MS. Differential electrophysiological changes in striatal output neurons in Huntington's disease. J Neurosci. 2011; 31:1170–1182. [PubMed: 21273402]

Arzberger T, Krampfl K, Leimgruber S, Weindl A. Changes of NMDA receptor subunit (NR1, NR2B) and glutamate transporter (GLT1) mRNA expression in Huntington's disease--an in situ hybridization study. J Neuropathol Exp Neurol. 1997; 56:440–454. [PubMed: 9100675]

Beal MF, Hyman BT, Koroshetz W. Do defects in mitochondrial energy metabolism underlie the pathology of neurodegenerative diseases? Trends Neurosci. 1993; 16:125–131. [PubMed: 7682343]

Berendse HW, Groenewegen HJ. Organization of the thalamostriatal projections in the rat, with special emphasis on the ventral striatum. J Comp Neurol. 1990; 299:187–228. [PubMed: 2172326]

Bonelli RM, Hofmann P. A systematic review of the treatment studies in Huntington's disease since 1990. Expert Opin Pharmacother. 2007; 8:141–153. [PubMed: 17257085]

Bradford J, Shin JY, Roberts M, Wang CE, Li XJ, Li S. Expression of mutant huntingtin in mouse brain astrocytes causes age-dependent neurological symptoms. Proc Natl Acad Sci U S A. 2009; 106:22480–22485. [PubMed: 20018729]

Brusa L, Orlacchio A, Moschella V, Iani C, Bernardi G, Mercuri NB. Treatment of the symptoms of Huntington's disease: preliminary results comparing aripiprazole and tetrabenazine. Mov Disord. 2009; 24:126–129. [PubMed: 19170197]

Cepeda C, Wu N, Andre VM, Cummings DM, Levine MS. The corticostriatal pathway in Huntington's disease. Prog Neurobiol. 2007; 81:253–271. [PubMed: 17169479]

Cepeda C, Hurst RS, Calvert CR, Hernandez-Echeagaray E, Nguyen OK, Jocoy E, Christian LJ, Ariano MA, Levine MS. Transient and progressive electrophysiological alterations in the corticostriatal pathway in a mouse model of Huntington's disease. J Neurosci. 2003; 23:961–969. [PubMed: 12574425]

Cummings DM, Cepeda C, Levine MS. Alterations in striatal synaptic transmission are consistent across genetic mouse models of Huntington's disease. ASN Neuro. 2010; 2:e00036. [PubMed: 20585470]

Deng YP, Reiner A. Cholinergic interneurons in the Q140 knock-in mouse model of Huntington's disease: Reductions in dendritic branching and thalamostriatal input. J Comp Neurol. 2016

Deng YP, Wong T, Bricker-Anthony C, Deng B, Reiner A. Loss of corticostriatal and thalamostriatal synaptic terminals precedes striatal projection neuron pathology in heterozygous Q140 Huntington's disease mice. Neurobiol Dis. 2013; 60:89–107. [PubMed: 23969239]

Deng YP, Albin RL, Penney JB, Young AB, Anderson KD, Reiner A. Differential loss of striatal projection systems in Huntington's disease: a quantitative immunohistochemical study. J Chem Neuroanat. 2004; 27:143–164. [PubMed: 15183201]

DiFiglia M. Excitotoxic injury of the neostriatum: a model for Huntington's disease. Trends Neurosci. 1990; 13:286–289. [PubMed: 1695405]

DiFiglia M, Sapp E, Chase K, Schwarz C, Meloni A, Young C, Martin E, Vonsattel JP, Carraway R, Reeves SA, et al. Huntingtin is a cytoplasmic protein associated with vesicles in human and rat brain neurons. Neuron. 1995; 14:1075–1081. [PubMed: 7748555]

Ding J, Peterson JD, Surmeier DJ. Corticostriatal and thalamostriatal synapses have distinctive properties. J Neurosci. 2008; 28:6483–6492. [PubMed: 18562619]

Dvorzhak A, Vagner T, Kirmse K, Grantyn R. Functional Indicators of Glutamate Transport in Single Striatal Astrocytes and the Influence of Kir4.1 in Normal and Huntington Mice. J Neurosci. 2016; 36:4959–4975. [PubMed: 27147650]

Ellender TJ, Huerta-Ocampo I, Deisseroth K, Capogna M, Bolam JP. Differential modulation of excitatory and inhibitory striatal synaptic transmission by histamine. J Neurosci. 2011; 31:15340–15351. [PubMed: 22031880]

Estrada-Sanchez AM, Montiel T, Segovia J, Massieu L. Glutamate toxicity in the striatum of the R6/2 Huntington's disease transgenic mice is age-dependent and correlates with decreased levels of glutamate transporters. Neurobiol Dis. 2009; 34:78–86. [PubMed: 19168136]

Faideau M, Kim J, Cormier K, Gilmore R, Welch M, Auregan G, Dufour N, Guillermier M, Brouillet E, Hantraye P, Deglon N, Ferrante RJ, Bonvento G. In vivo expression of polyglutamine-expanded

Author Manuscript Author Manuscript Author Manuscript Author Manuscript

huntingtin by mouse striatal astrocytes impairs glutamate transport: a correlation with Huntington's disease subjects. Hum Mol Genet. 2010; 19:3053–3067. [PubMed: 20494921]

Fasano A, Cadeddu F, Guidubaldi A, Piano C, Soleti F, Zinzi P, Bentivoglio AR. The long-term effect of tetrabenazine in the management of Huntington disease. Clin Neuropharmacol. 2008; 31:313–318. [PubMed: 19050408]

Franklin, KBJ., Paxinos, G. The Mouse Brain in Stereotaxic Coordinates. 3. Academic Press; 2007.

Freese A, DiFiglia M, Koroshetz WJ, Beal MF, Martin JB. Characterization and mechanism of glutamate neurotoxicity in primary striatal cultures. Brain Res. 1990; 521:254–264. [PubMed: 1976413]

Fremeau RT Jr, Troyer MD, Pahner I, Nygaard GO, Tran CH, Reimer RJ, Bellocchio EE, Fortin D, Storm-Mathisen J, Edwards RH. The expression of vesicular glutamate transporters defines two classes of excitatory synapse. Neuron. 2001; 31:247–260. [PubMed: 11502256]

Galvan L, Andre VM, Wang EA, Cepeda C, Levine MS. Functional Differences Between Direct and Indirect Striatal Output Pathways in Huntington's Disease. J Huntingtons Dis. 2012; 1:17–25. [PubMed: 25063187]

Gerfen CR, Engber TM, Mahan LC, Susel Z, Chase TN, Monsma FJ Jr, Sibley DR. D1 and D2 dopamine receptor-regulated gene expression of striatonigral and striatopallidal neurons. Science. 1990; 250:1429–1432. [PubMed: 2147780]

Graham RK, Pouladi MA, Joshi P, Lu G, Deng Y, Wu NP, Figueroa BE, Metzler M, Andre VM, Slow EJ, Raymond L, Friedlander R, Levine MS, Leavitt BR, Hayden MR. Differential Susceptibility to Excitotoxic Stress in YAC128 Mouse Models of Huntington Disease between Initiation and Progression of Disease. J Neurosci. 2009; 29:2193–2204. [PubMed: 19228972]

Harper, PS., Jones, L. Huntington's disease: Genetic and molecular studies. In: Bates, GP.Harper, PS., Jones, L., editors. Huntington's Disease. 3. Oxford: Oxford University Press; 2002. p. 113-158.

Hassel B, Tessler S, Faull RL, Emson PC. Glutamate uptake is reduced in prefrontal cortex in Huntington's disease. Neurochem Res. 2008; 33:232–237. [PubMed: 17726644]

Heinsen H, Rub U, Gangnus D, Jungkunz G, Bauer M, Ulmar G, Bethke B, Schuler M, Bocker F, Eisenmenger W, Gotz M, Strik M. Nerve cell loss in the thalamic centromedian-parafascicular complex in patients with Huntington's disease. Acta Neuropathol. 1996; 91:161–168. [PubMed: 8787149]

Herzog E, Bellenchi GC, Gras C, Bernard V, Ravassard P, Bedet C, Gasnier B, Giros B, El Mestikawy S. The existence of a second vesicular glutamate transporter specifies subpopulations of glutamatergic neurons. J Neurosci. 2001; 21:RC181. [PubMed: 11698619]

Hoffner G, Kahlem P, Djian P. Perinuclear localization of huntingtin as a consequence of its binding to microtubules through an interaction with beta-tubulin: relevance to Huntington's disease. J Cell Sci. 2002; 115:941–948. [PubMed: 11870213]

Horikawa K, Armstrong WE. A versatile means of intracellular labeling: injection of biocytin and its detection with avidin conjugates. J Neurosci Methods. 1988; 25:1–11. [PubMed: 3146670]

Huerta-Ocampo I, Mena-Segovia J, Bolam JP. Convergence of cortical and thalamic input to direct and indirect pathway medium spiny neurons in the striatum. Brain Struct Funct. 2014; 219:1787–1800. [PubMed: 23832596]

Hunnicutt BJ, Jongbloets BC, Birdsong WT, Gertz KJ, Zhong H, Mao T. A comprehensive excitatory input map of the striatum reveals novel functional organization. Elife. 2016:5.

Indersmitten T, Tran CH, Cepeda C, Levine MS. Altered excitatory and inhibitory inputs to striatal medium-sized spiny neurons and cortical pyramidal neurons in the Q175 mouse model of Huntington's disease. J Neurophysiol. 2015; 113:2953–2966. [PubMed: 25673747]

Joshi PR, Wu NP, Andre VM, Cummings DM, Cepeda C, Joyce JA, Carroll JB, Leavitt BR, Hayden MR, Levine MS, Bamford NS. Age-dependent alterations of corticostriatal activity in the YAC128 mouse model of Huntington disease. J Neurosci. 2009; 29:2414–2427. [PubMed: 19244517]

Kassubek J, Gaus W, Landwehrmeyer GB. Evidence for more widespread cerebral pathology in early HD: an MRI-based morphometric analysis. Neurology. 2004; 62:523–524. author reply 524.

Kassubek J, Juengling FD, Ecker D, Landwehrmeyer GB. Thalamic atrophy in Huntington's disease co-varies with cognitive performance: a morphometric MRI analysis. Cereb Cortex. 2005; 15:846–853. [PubMed: 15459079]

Author Manuscript Author Manuscript Author Manuscript Author Manuscript

Klapstein GJ, Fisher RS, Zanjani H, Cepeda C, Jokel ES, Chesselet MF, Levine MS. Electrophysiological and Morphological Changes in Striatal Spiny Neurons in R6/2 Huntington's Disease Transgenic Mice. J Neurophysiol. 2001; 86:2667–2677. [PubMed: 11731527]

Kolodziejczyk K, Raymond LA. Differential changes in thalamic and cortical excitatory synapses onto striatal spiny projection neurons in a Huntington disease mouse model. Neurobiol Dis. 2016; 86:62–74. [PubMed: 26621114]

Lei W, Jiao Y, Del Mar N, Reiner A. Evidence for differential cortical input to direct pathway versus indirect pathway striatal projection neurons in rats. J Neurosci. 2004; 24:8289–8299. [PubMed: 15385612]

Li H, Wyman T, Yu ZX, Li SH, Li XJ. Abnormal association of mutant huntingtin with synaptic vesicles inhibits glutamate release. Hum Mol Genet. 2003; 12:2021–2030. [PubMed: 12913073]

Lievens JC, Woodman B, Mahal A, Spasic-Boscovic O, Samuel D, Kerkerian-Le Goff L, Bates GP. Impaired glutamate uptake in the R6 Huntington's disease transgenic mice. Neurobiol Dis. 2001; 8:807–821. [PubMed: 11592850]

Meshul CK, Stallbaumer RK, Taylor B, Janowsky A. Haloperidol-induced morphological changes in striatum are associated with glutamate synapses. Brain Res. 1994; 648:181–195. [PubMed: 7922533]

Meshul CK, Emre N, Nakamura CM, Allen C, Donohue MK, Buckman JF. Time-dependent changes in striatal glutamate synapses following a 6-hydroxydopamine lesion. Neuroscience. 1999; 88:1–16. [PubMed: 10051185]

Mestre T, Ferreira J, Coelho MM, Rosa M, Sampaio C. Therapeutic interventions for symptomatic treatment in Huntington's disease. Cochrane Database Syst Rev. 2009:CD006456. [PubMed: 19588393]

Miller BR, Dorner JL, Shou M, Sari Y, Barton SJ, Sengelaub DR, Kennedy RT, Rebec GV. Up-regulation of GLT1 expression increases glutamate uptake and attenuates the Huntington's disease phenotype in the R6/2 mouse. Neuroscience. 2008; 153:329–337. [PubMed: 18353560]

NicNiocaill B, Haraldsson B, Hansson O, O'Connor WT, Brundin P. Altered striatal amino acid neurotransmitter release monitored using microdialysis in R6/1 Huntington transgenic mice. Eur J Neurosci. 2001; 13:206–210. [PubMed: 11135020]

Parsons MP, Vanni MP, Woodard CL, Kang R, Murphy TH, Raymond LA. Real-time imaging of glutamate clearance reveals normal striatal uptake in Huntington disease mouse models. Nat Commun. 2016; 7:11251. [PubMed: 27052848]

Phend KD, Weinberg RJ, Rustioni A. Techniques to optimize post-embedding single and double staining for amino acid neurotransmitters. J Histochem Cytochem. 1992; 40:1011–1020. [PubMed: 1376741]

Raymond LA, André VM, Cepeda C, Gladding CM, Milnerwood AJ, Levine MS. Pathophysiology of Huntington's disease: time-dependent alterations in synaptic and receptor function. Neuroscience. 2011

Reiner A, Albin RL, Anderson KD, D'Amato CJ, Penney JB, Young AB. Differential loss of striatal projection neurons in Huntington disease. Proc Natl Acad Sci U S A. 1988; 85:5733–5737. [PubMed: 2456581]

Sadikot AF, Parent A, Francois C. Efferent connections of the centromedian and parafascicular thalamic nuclei in the squirrel monkey: a PHA-L study of subcortical projections. J Comp Neurol. 1992; 315:137–159. [PubMed: 1372010]

Sciamanna G, Ponterio G, Mandolesi G, Bonsi P, Pisani A. Optogenetic stimulation reveals distinct modulatory properties of thalamostriatal vs corticostriatal glutamatergic inputs to fast-spiking interneurons. Sci Rep. 2015; 5:16742. [PubMed: 26572101]

Sesack SR, Aoki C, Pickel VM. Ultrastructural localization of D2 receptor-like immunoreactivity in midbrain dopamine neurons and their striatal targets. J Neurosci. 1994; 14:88–106. [PubMed: 7904306]

Shimamoto K, Sakai R, Takaoka K, Yumoto N, Nakajima T, Amara SG, Shigeri Y. Characterization of novel L-threo-beta-benzyloxyaspartate derivatives, potent blockers of the glutamate transporters. Mol Pharmacol. 2004; 65:1008–1015. [PubMed: 15044631]

Author Manuscript Author Manuscript Author Manuscript Author Manuscript

Sidibe M, Smith Y. Differential synaptic innervation of striatofugal neurones projecting to the internal or external segments of the globus pallidus by thalamic afferents in the squirrel monkey. J Comp Neurol. 1996; 365:445–465. [PubMed: 8822181]

Singaraja RR, Huang K, Sanders SS, Milnerwood AJ, Hines R, Lerch JP, Franciosi S, Drisdel RC, Vaid K, Young FB, Doty C, Wan J, Bissada N, Henkelman RM, Green WN, Davis NG, Raymond LA, Hayden MR. Altered palmitoylation and neuropathological deficits in mice lacking HIP14. Hum Mol Genet. 2011; 20:3899–3909. [PubMed: 21775500]

Smeal RM, Keefe KA, Wilcox KS. Differences in excitatory transmission between thalamic and cortical afferents to single spiny efferent neurons of rat dorsal striatum. Eur J Neurosci. 2008; 28:2041–2052. [PubMed: 19046385]

Smeal RM, Gaspar RC, Keefe KA, Wilcox KS. A rat brain slice preparation for characterizing both thalamostriatal and corticostriatal afferents. J Neurosci Methods. 2006

Smith AD, Bolam JP. The neural network of the basal ganglia as revealed by the study of synaptic connections of identified neurones. Trends Neurosci. 1990; 13:259–265. [PubMed: 1695400]

Smith Y, Raju DV, Pare JF, Sidibe M. The thalamostriatal system: a highly specific network of the basal ganglia circuitry. Trends Neurosci. 2004; 27:520–527. [PubMed: 15331233]

Smith Y, Galvan A, Ellender TJ, Doig N, Villalba RM, Huerta-Ocampo I, Wichmann T, Bolam JP. The thalamostriatal system in normal and diseased states. Front Syst Neurosci. 2014; 8:5. [PubMed: 24523677]

Spinelli KJ, Taylor JK, Osterberg VR, Churchill MJ, Pollock E, Moore C, Meshul CK, Unni VK. Presynaptic alpha-synuclein aggregation in a mouse model of Parkinson's disease. J Neurosci. 2014; 34:2037–2050. [PubMed: 24501346]

Steiner H, Gerfen CR. Enkephalin regulates acute D2 dopamine receptor antagonist-induced immediate-early gene expression in striatal neurons. Neuroscience. 1999; 88:795–810. [PubMed: 10363818]

The Huntington's Disease Collaborative Research Group. A novel gene containing a trinucleotide repeat that is expanded and unstable on Huntington's disease chromosomes. Cell. 1993; 72:971–983. [PubMed: 8458085]

Tong X, Ao Y, Faas GC, Nwaobi SE, Xu J, Haustein MD, Anderson MA, Mody I, Olsen ML, Sofroniew MV, Khakh BS. Astrocyte Kir4.1 ion channel deficits contribute to neuronal dysfunction in Huntington's disease model mice. Nat Neurosci. 2014

Velier J, Kim M, Schwarz C, Kim TW, Sapp E, Chase K, Aronin N, DiFiglia M. Wild-type and mutant huntingtins function in vesicle trafficking in the secretory and endocytic pathways. Exp Neurol. 1998; 152:34–40. [PubMed: 9682010]

Vonsattel JP, Myers RH, Stevens TJ, Ferrante RJ, Bird ED, Richardson EP Jr. Neuropathological classification of Huntington's disease. J Neuropathol Exp Neurol. 1985; 44:559–577. [PubMed: 2932539]

Waelter S, Scherzinger E, Hasenbank R, Nordhoff E, Lurz R, Goehler H, Gauss C, Sathasivam K, Bates GP, Lehrach H, Wanker EE. The huntingtin interacting protein HIP1 is a clathrin and alpha-adaptin-binding protein involved in receptor-mediated endocytosis. Hum Mol Genet. 2001; 10:1807–1817. [PubMed: 11532990]

Walker RH, Moore C, Davies G, Dirling LB, Koch RJ, Meshul CK. Effects of subthalamic nucleus lesions and stimulation upon corticostriatal afferents in the 6-hydroxydopamine-lesioned rat. PLoS One. 2012; 7:e32919. [PubMed: 22427909]

Wang N, Gray M, Lu XH, Cantle JP, Holley SM, Greiner E, Gu X, Shirasaki D, Cepeda C, Li Y, Dong H, Levine MS, Yang XW. Neuronal targets for reducing mutant huntingtin expression to ameliorate disease in a mouse model of Huntington's disease. Nat Med. 2014; 20:536–541. [PubMed: 24784230]

Zuccato C, Ciammola A, Rigamonti D, Leavitt BR, Goffredo D, Conti L, MacDonald ME, Friedlander RM, Silani V, Hayden MR, Timmusk T, Sipione S, Cattaneo E. Loss of huntingtin-mediated BDNF gene transcription in Huntington's disease. Science. 2001; 293:493–498. [PubMed: 11408619]

Zucker RS. Short-term synaptic plasticity. Annu Rev Neurosci. 1989; 12:13–31. [PubMed: 2648947]

Author Manuscript Author Manuscript Author Manuscript Author Manuscript

Highlights

- Optogenetics, slice electrophysiology, and electron microscopy, were used to examine morphological and electrophysiological changes in corticostriatal and thalamostriatal projections in a mouse model of Huntington's disease.
- In symptomatic R6/2 mice corticostriatal glutamate receptor-mediated responses were reduced. Although thalamostriatal responses also were reduced, the areas remained unchanged due to an increase in decay times.
- The probability of glutamate release was higher at thalamostriatal than corticostriatal synapses, particularly in R6/2 mice.
- Morphological studies indicated that the density of all excitatory synaptic contacts onto MSNs was reduced. There was a consistent reduction in the area of spines but little change in presynaptic terminal size.
- These results highlight the significant and differential contribution of the thalamostriatal projection to glutamate excitotoxicity in HD.

Author Manuscript Author Manuscript Author Manuscript Author Manuscript

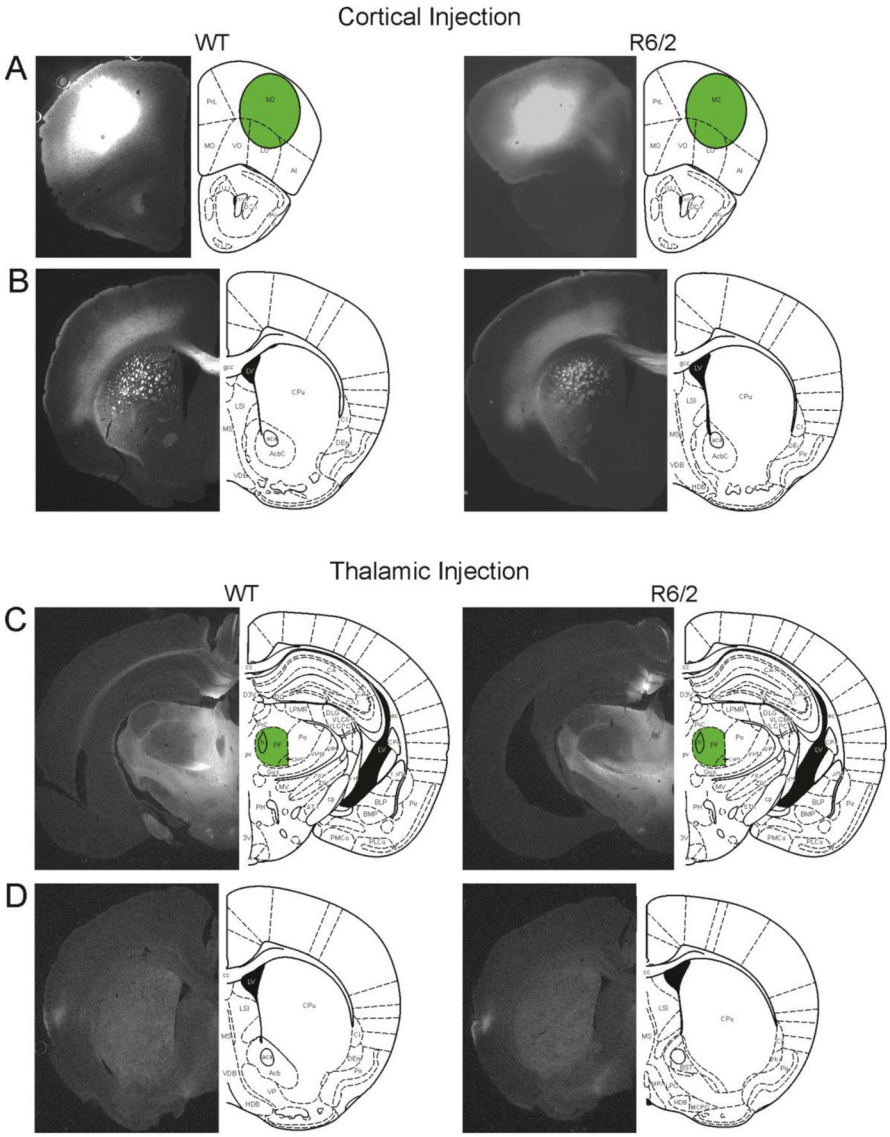

Fig. 1.

A. Typical YFP expression patterns at the injection site following AAV-CaMKIIa-YFP-ChR2 virus injections into the cortex of a WT (left) and an R6/2 (right) mouse. **B.** Typical YFP expression pattern in the corresponding striatum of the same mice in A. **C.** Typical YFP expression patterns at the injection site following viral injection into the CM/Pf of a WT (left) and an R6/2 (right) mouse. **D.** Typical YFP expression patterns in the corresponding striatum of the same mice in C.

Author Manuscript Author Manuscript Author Manuscript Author Manuscript

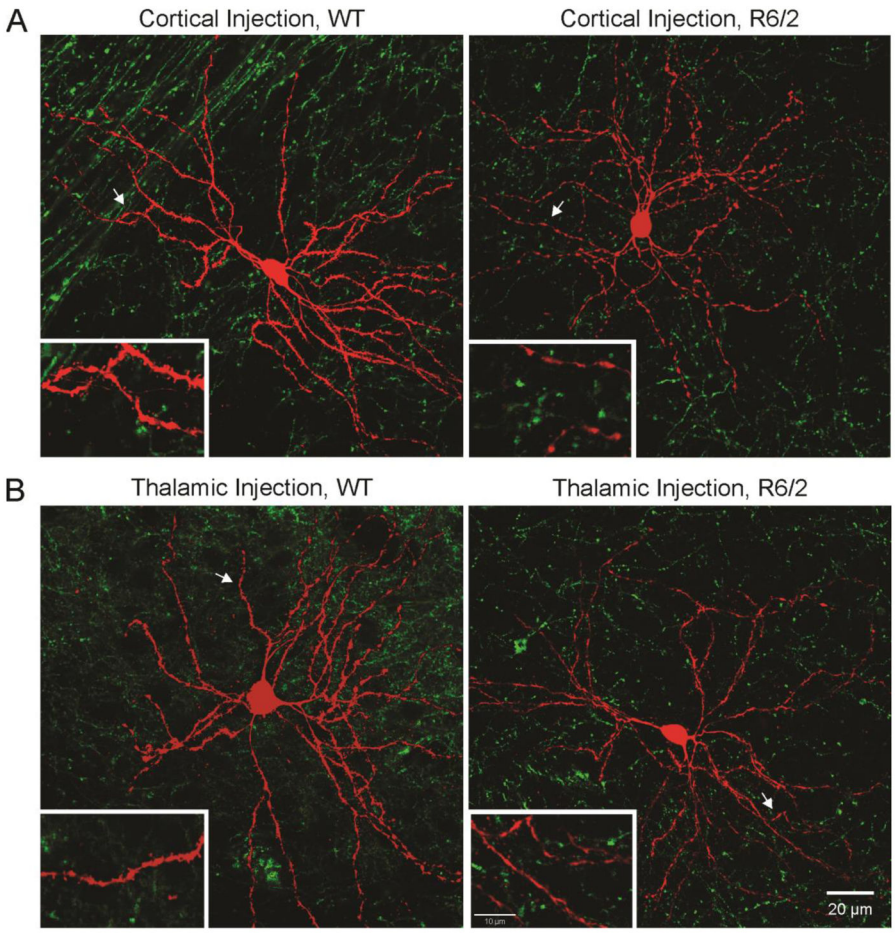

Fig. 2.

Fluorescent confocal microscope images of biocytin-filled MSNs (in red) during electrophysiological recordings and striatal ChR2 axonal expression (in green) in WT and R6/2 mice after cortical **(A)** or thalamic **(B)** viral injection. Calibration bar applies to all panels. Insets show a magnified segment of dendrites and spines. Calibration bar in the bottom right inset applies to all insets.

Author Manuscript Author Manuscript Author Manuscript Author Manuscript

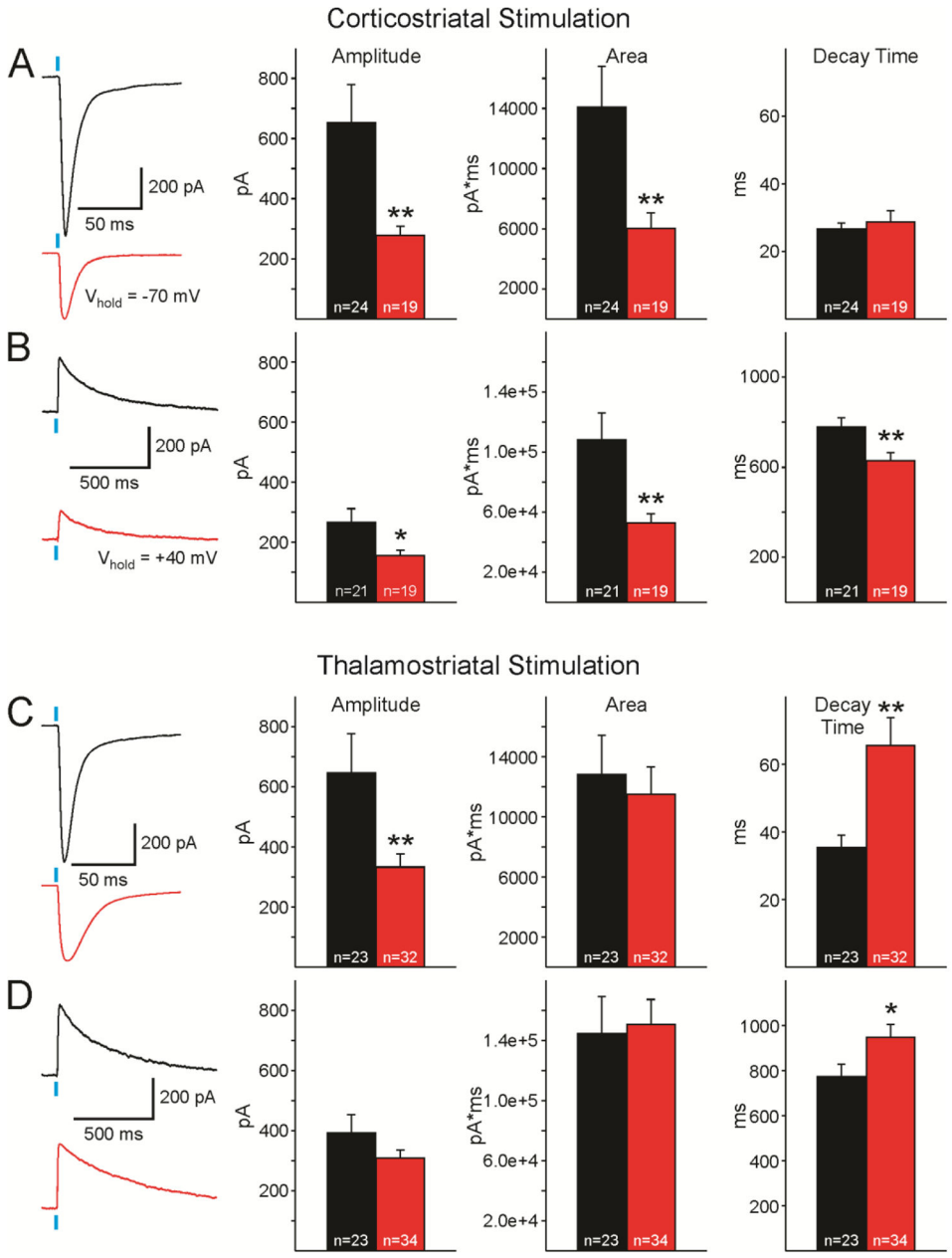

Fig. 3.

A. AMPAR-mediated currents evoked by corticostriatal stimulation. Left panels show representative sample traces of AMPAR-mediated responses recorded in an MSN from a WT (black) and an R6/2 (red). Graphs on the right show average amplitudes, areas, and decay times (±SEM) of AMPAR-mediated responses evoked by corticostriatal stimulation. **B.** NMDAR-mediated currents evoked by corticostriatal stimulation. Representative sample traces of AMPAR-mediated responses recorded in an MSN from a WT and an R6/2. Graphs indicate average amplitudes, areas, and decay times (±SEM) of NMDAR-mediated responses evoked by corticostriatal stimulation. **C.** AMPAR-mediated currents evoked by thalamostriatal stimulation. Left panels show representative sample traces of AMPAR-

Author Manuscript Author Manuscript Author Manuscript Author Manuscript

mediated responses recorded in an MSN from a WT mouse and R6/2 mouse. Graphs show average amplitudes, areas, and decay times (±SEM) of AMPAR-mediated responses evoked by thalamostriatal stimulation. **D.** NMDAR-mediated currents evoked by thalamostriatal stimulation. Left panels show representative sample traces of AMPAR-mediated responses recorded in an MSN from a WT and an R6/2. Graphs show average amplitudes, areas, and decay times (±SEM) of NMDAR-mediated responses evoked by thalamostriatal stimulation. In this and all other figures, Ns are shown in each bar and asterisks in this and subsequent figures indicate * $p<0.05$, ** $p<0.01$, *** $p<0.001$.

Author Manuscript Author Manuscript Author Manuscript Author Manuscript

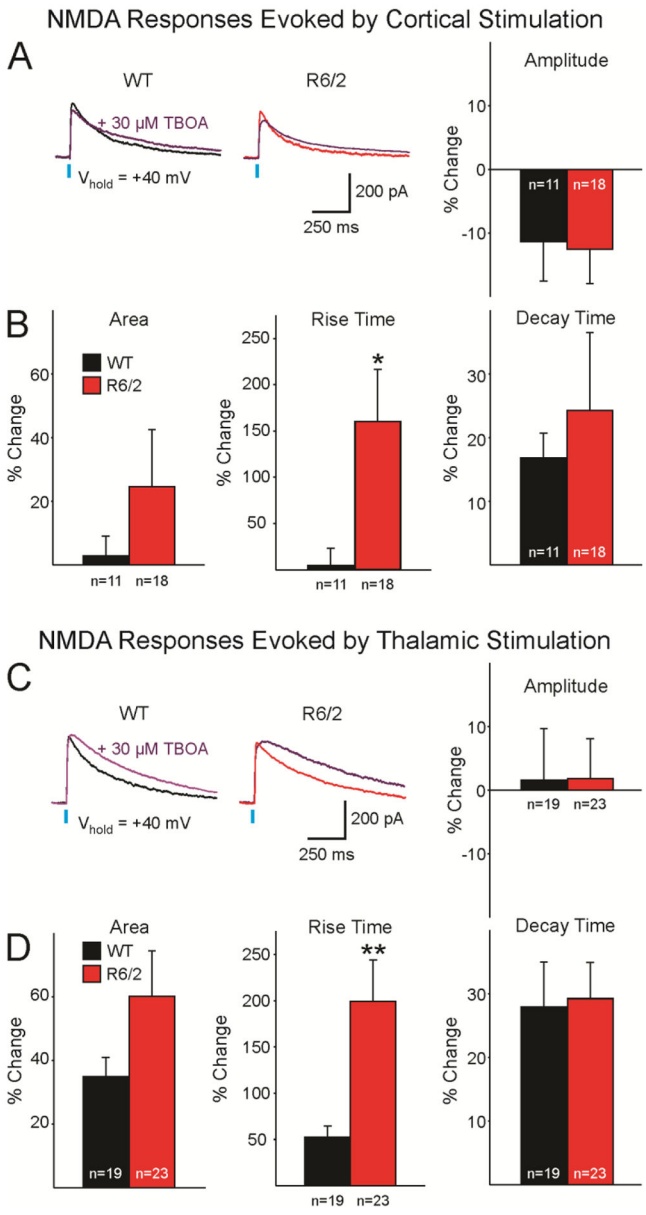

Fig. 4.

A. Representative sample traces of NMDAR-mediated responses evoked by corticostriatal stimulation, recorded in an MSN from a WT (black) and an R6/2 (red), before and after TBOA application (purple). Graph on the right shows average percent change of amplitude (±SEM). **B.** Average percent changes in area, rise time, and decay time (±) of NMDAR-mediated currents evoked by corticostriatal stimulation 14 min post bath application of TBOA. **C.** Representative sample traces of NMDAR-mediated responses evoked by thalamostriatal stimulation, recorded in an MSN from a WT and an R6/2, before and after TBOA application. Graph on the right shows average percent change of amplitude (±SEM). **D.** Average percent changes in area, rise time, and decay time (±SEM) of NMDAR-mediated currents evoked by thalamostriatal stimulation 14 min post bath application of TBOA.

Author Manuscript Author Manuscript Author Manuscript Author Manuscript

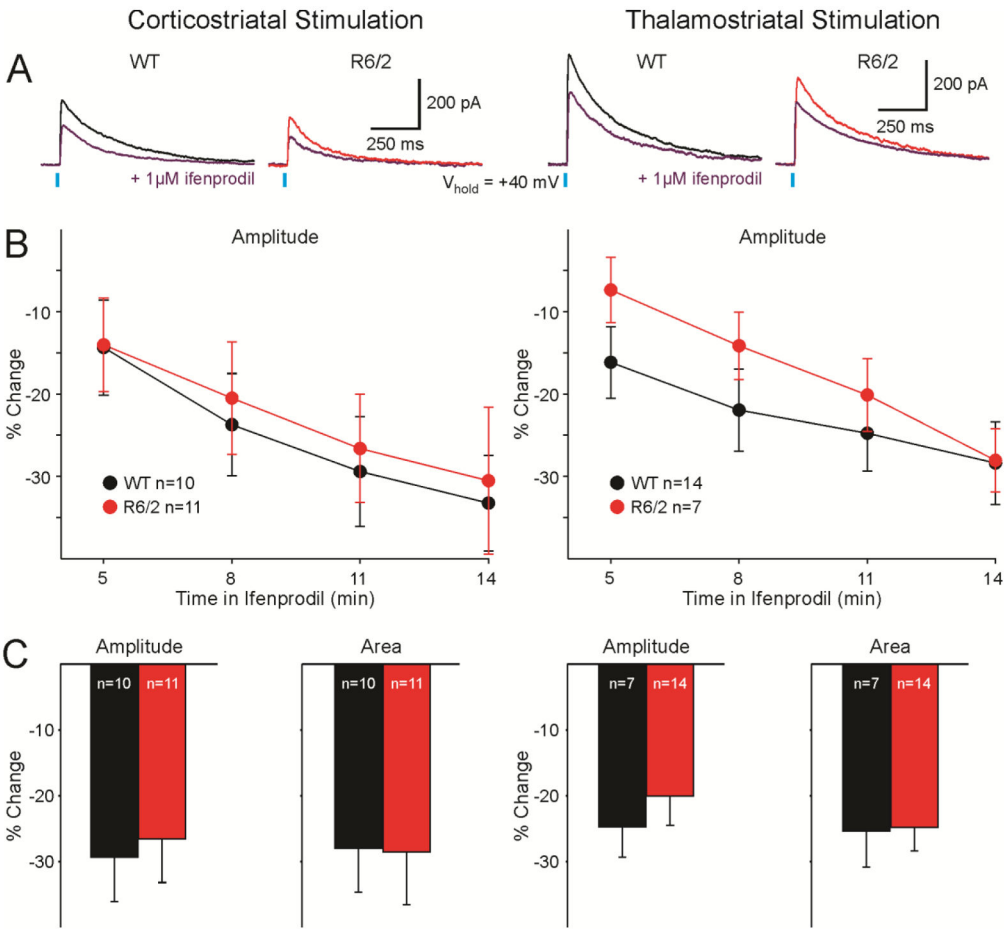

Fig. 5.

A. Representative sample traces of NMDAR-mediated responses evoked by corticostriatal (left) and thalamostriatal (right) stimulation, recorded in MSNs from a WT (black) and an R6/2 (red) before and after bath application of Ifenprodil (purple). **B.** Average percent change of amplitudes (±SEM) of NMDAR-mediated currents over time evoked by corticostriatal (left) and thalamostriatal (right) stimulation. **C.** Average percent change of amplitudes and areas (±SEM) of NMDAR-mediated currents evoked by corticostriatal (left) and thalamostriatal (right) stimulation 11 min post bath application of Ifenprodil.

Author Manuscript Author Manuscript Author Manuscript Author Manuscript

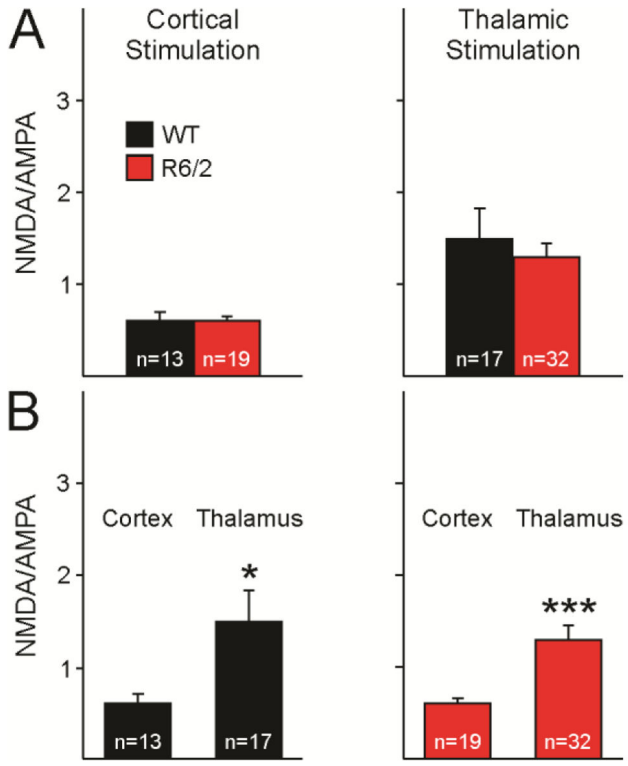

Fig. 6.

A. NMDA/AMPA ratios evoked by corticostriatal (left) and thalamostriatal (right) stimulation. Peak amplitude of the NMDAR-mediated current was divided by the amplitude of the AMPAR-mediated current evoked by corticostriatal or thalamostriatal stimulation for each neuron, and then averaged across neurons. **B.** NMDA/AMPA ratios of currents evoked by corticostriatal stimulation compared to those evoked by thalamostriatal stimulation in MSNs from WT (left) and R6/2 (right).

Author Manuscript Author Manuscript Author Manuscript Author Manuscript

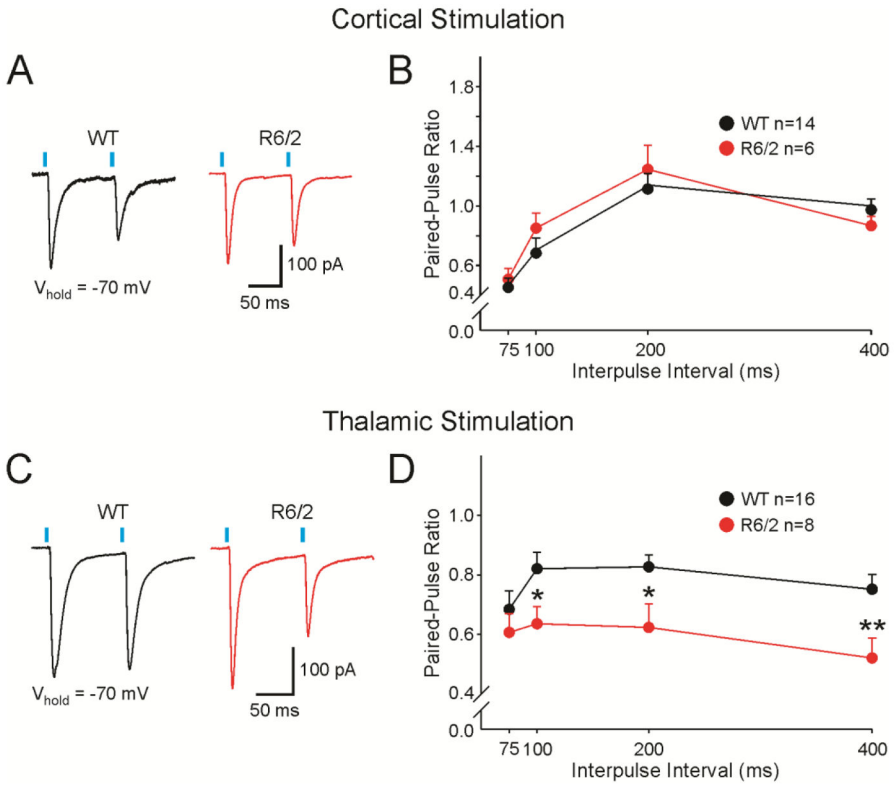

Fig. 7.

A. Representative sample traces (100 ms inter-pulse interval) and average paired-pulse ratios ±SEM **(B)** of AMPAR-mediated EPSCs evoked by corticostriatal stimulation at V_{hold}=−70 mV. **C.** Representative sample traces (100 ms pulse inter-pulse interval) and average paired-pulse ratios±SEM **(D)** of AMPAR-mediated EPSCs evoked by thalamostriatal stimulation at V_{hold}=−70 mV.

Author Manuscript Author Manuscript Author Manuscript Author Manuscript

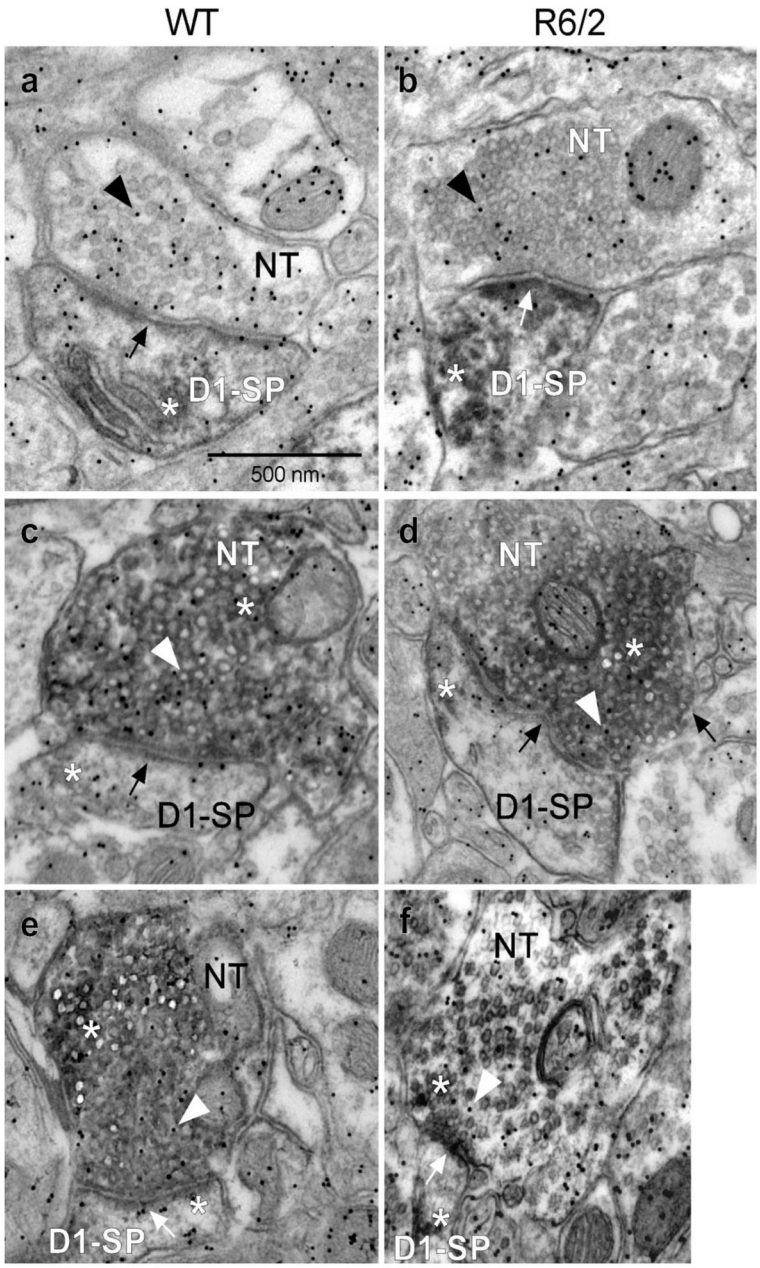

Fig. 8.

VGLUT1/VGLUT2 terminal input onto D1R labeled spines (D1-SP) within the dorsolateral striatum. Electron photomicrographs showing single DAB labeling for D1Rs only within spines (panels **a** and **b**, respectively), VGLUT1 and VGLUT2 labeling within nerve terminals (NT), along with nerve terminal glutamate immuno-gold labeling (arrowhead within the nerve terminal). White asterisk shows DAB label and black or white arrows indicate synapse. **a:** D1R-labeled spine, WT; **b:** D1R-labeled spine, R6/2; **c:** D1R-labeled spine and VGLUT1 labeled terminal, WT; **d:** D1R-labeled spine and VGLUT1 labeled terminal, R6/2; **e:** D1R labeled spine and VGLUT2 labeled terminal, WT; **f:** D1R labeled spine and VGLUT2 labeled terminal, R6/2. Calibration bar: 500 nm.

Author Manuscript Author Manuscript Author Manuscript Author Manuscript

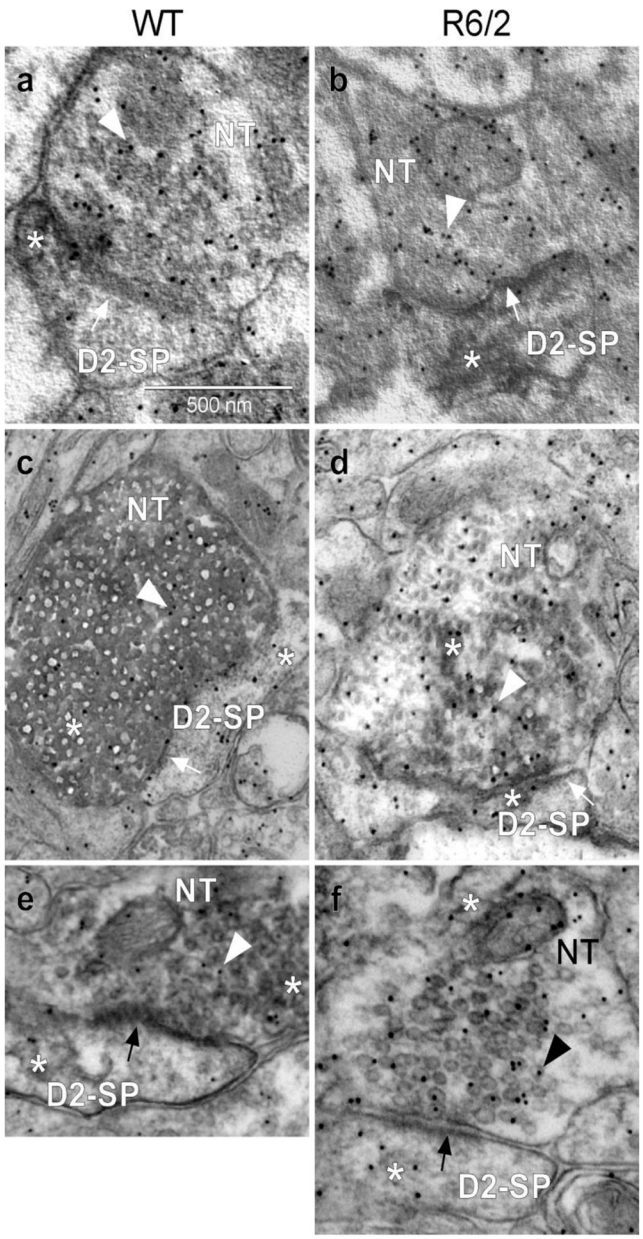

Fig. 9.

VGLUT1/VGLUT2 terminal input onto D2R-labeled spines (D2-SP) within the dorsolateral striatum. Electron photomicrographs showing single DAB labeling for D2R only within spines (panels **a** and **b**, WT and R6/2, respectively), VGLUT1 (panels **c** and **d**) and VGLUT2 (panels **e** and **f**) labeling within nerve terminals (NT), along with nerve terminal glutamate immuno-gold labeling (arrowhead within the nerve terminal). Synaptic contacts (arrows) are illustrated. White asterisk shows DAB label, black or white arrows indicate synapse, arrowheads indicate gold particle, NT is the nerve terminal, while SP is the spine. **a:** D2R-labeled spine, WT; **b:** D2R-labeled spine, R6/2; **c:** D2R-labeled spine and VGLUT1 labeled terminal, WT; **d:** D2R-labeled spine and VGLUT1 labeled terminal, R6/2; **e:** D2R-

Author Manuscript Author Manuscript Author Manuscript Author Manuscript

labeled spine and VGLUT2 labeled terminal, WT; **f:** D2R-labeled spine and VGLUT2 labeled terminal, R6/2. Calibration bar: 500 nm.

Author Manuscript Author Manuscript Author Manuscript Author Manuscript

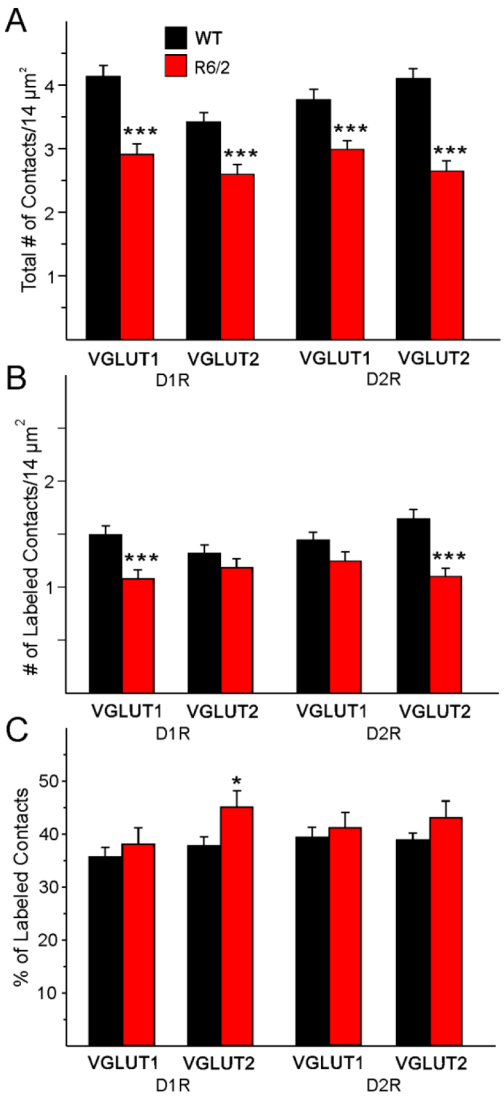

Fig. 10.

A. Mean (±SEM) of the number of total contacts per field of view (14 µm^2) for all contacts regardless of whether they originated from cortex (VGLUT1) onto both D1R- and D2R-expressing spines or from thalamus (VGLUT2) onto both D1R- and D2R-expressing spines in WT (n=7) and R6/2 (n=9) littermates. **B.** Mean (±SEM) of the number of labeled contacts per field of view (14 µm^2) for just VGLUT1 and VGLUT2 contacts onto only D1R- and D2R-expressing spines. **C.** Mean (±SEM) of the percent of labeled contacts for VGLUT1 and VGLUT2 contacts on D1R- and D2R-expressing spines.

Author Manuscript Author Manuscript Author Manuscript Author Manuscript

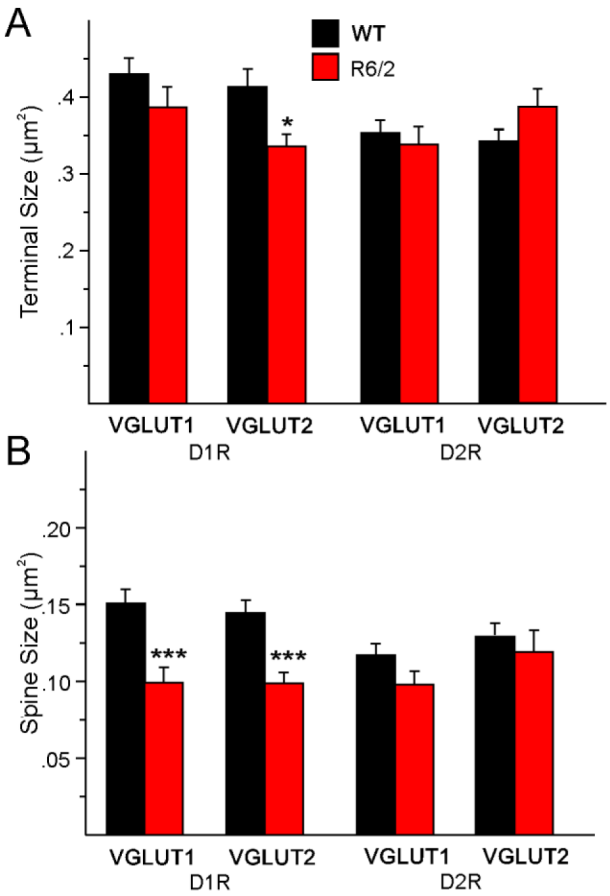

Fig. 11.

A. Mean (±SEM) of the area of terminal size for all terminals from cortex (VGLUT1) onto both D1R- and D2R-expressing spines and from thalamus (VGLUT2) onto both D1R- and D2R-expressing spines in WT (n=7) and R6/2 (n=9) littermates. **B.** Mean (±SEM) of the areas of all D1R- and D2R-expressing spines were reduced in R6/2 mice.

Author Manuscript Author Manuscript Author Manuscript Author Manuscript

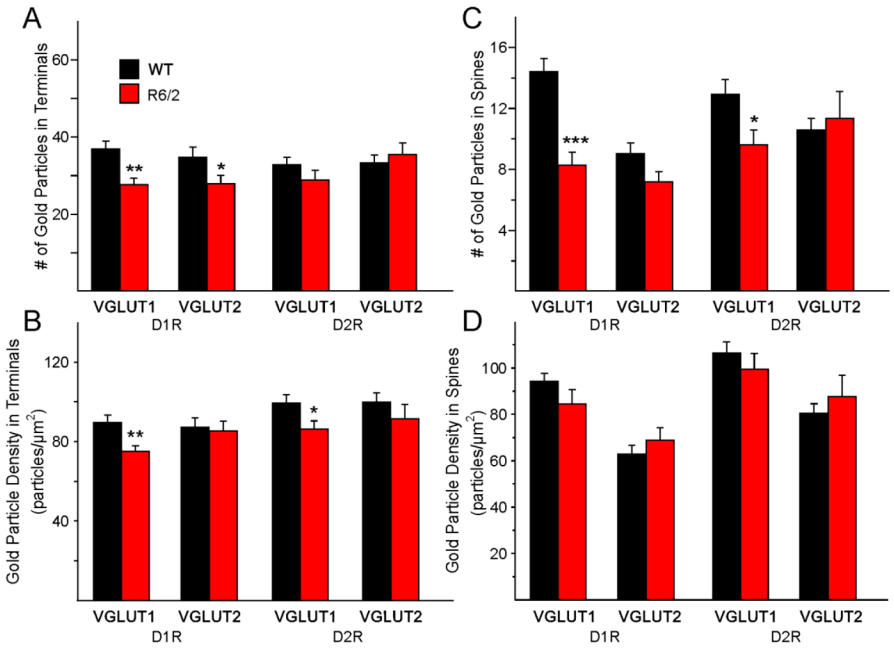

Fig. 12.

A. Mean (±SEM) numbers of gold particles in VGLUT1 and VGLUT2 terminals contacting spines expressing D1Rs or D2Rs in WT (n=7) and R6/2 (n=9) littermates. **B.** Mean (±SEM) density of gold particles in VGLUT1 and VGLUT2 terminals contacting spines expressing D1Rs or D2Rs. **C.** Mean (±SEM) numbers of gold particles in VGLUT1 and VGLUT2 terminals. **D.** Mean (±SEM) density of gold particles in spines expressing D1Rs or D2Rs and contacted by VGLUT1 and VGLUT2 terminals.

Author Manuscript

Author Manuscript

Author Manuscript

Author Manuscript

Table 1

Passive membrane properties of MSNs from WT and R6/2 mice

	WT	R6/2
Cm (pF)	97.96 ± 3.84 (50)	77.91 ± 1.82 (62) ***
Rm (MΩ)	64.52 ± 4.27 (47)	162.06 ± 9.94 (58) ***
Tau (ms)	1.78 ± 0.46 (50)	1.68 ± 0.06 (62)
Hold (pA)	−91.97 ± 53.47 (50)	−41.15 ± 3.79 (62) ***

Numbers in parentheses indicate the number of MSNs recorded. Values are means ± S.E.M.

*** indicates statistical significance of $p<0.001$